



HAL
open science

Young Martian crater Gratteri and its secondary craters

Cathy Quantin, Olga Popova, William K. Hartmann, Stephanie C. Werner

► To cite this version:

Cathy Quantin, Olga Popova, William K. Hartmann, Stephanie C. Werner. Young Martian crater Gratteri and its secondary craters. *Journal of Geophysical Research. Planets*, 2016, 121 (7), pp.1118-1140. 10.1002/2015JE004864 . hal-02331145

HAL Id: hal-02331145

<https://univ-lyon1.hal.science/hal-02331145>

Submitted on 13 Sep 2021

HAL is a multi-disciplinary open access archive for the deposit and dissemination of scientific research documents, whether they are published or not. The documents may come from teaching and research institutions in France or abroad, or from public or private research centers.

L'archive ouverte pluridisciplinaire **HAL**, est destinée au dépôt et à la diffusion de documents scientifiques de niveau recherche, publiés ou non, émanant des établissements d'enseignement et de recherche français ou étrangers, des laboratoires publics ou privés.

Copyright

RESEARCH ARTICLE

10.1002/2015JE004864

Young Martian crater Gratteri and its secondary craters

Cathy Quantin¹, Olga Popova², William K. Hartmann³, and Stephanie C. Werner⁴

Key Points:

- We studied properties of the secondary crater field around the young primary ray crater Gratteri
- Crater density in rays tends to peak around 120–230 km from Gratteri
- In old terrains, secondaries have minimal effect on crater chronometry

Supporting Information:

- Supporting Information S1

Correspondence to:

C. Quantin,
quantin@univ-lyon1.fr

Citation:

Quantin, C., O. Popova, W. K. Hartmann, and S. C. Werner (2016), Young Martian crater Gratteri and its secondary craters, *J. Geophys. Res. Planets*, 121, 1118–1140, doi:10.1002/2015JE004864.

Received 5 JUN 2015

Accepted 4 JUN 2016

Accepted article online 8 JUN 2016

Published online 2 JUL 2016

¹Laboratoire de géologie de Lyon: Terre, Planètes, Environnements, Université Lyon 1/Ecole Normale Supérieure de Lyon/CNRS, UMR 5276, Villeurbanne, France, ²Institute for Dynamics of Geospheres, Moscow, Russia, ³Planetary Science Institute, Tucson, Arizona, USA, ⁴Centre for Earth Evolution and Dynamics, Department for Geosciences, University of Oslo, Oslo, Norway

Abstract In response to questions that have been raised about formation and effects of secondary craters on crater chronometry techniques, we studied properties of the secondary crater field around the young Martian primary ray crater Gratteri (diameter 7 km). The crater has an estimated age of 1 to 20 Myr, based on counts of small craters on flat interior surface, consistent with a likely age for a young crater its size (Hartmann et al., 2010). The following are among our findings: (1) We identify an unusual class of craters we call “rampart secondaries” which may suggest low-angle impacts. (2) We measure size distributions of secondaries as a function of distance from Gratteri and used these data to reconstruct the mass-velocity distribution of ejecta blasted out of Gratteri. Our data suggest that crater density in rays tends to peak around 120–230 km from Gratteri (roughly 20–30D) and reaches roughly 30–70 times the interray crater density. (3) Comparable total numbers of secondaries form inside rays and outside rays, and about half are concentrated in clusters in 2% of the area around Gratteri, with the others scattered over 98% of the area out to 400 km away from Gratteri. (4) In the old Noachian plains around Gratteri, secondaries have minimal effect on crater chronometry. These results, along with recently reported direct measurements of the rate of formation of 10 m to 20 m primaries on Mars (Daubar et al., 2013), tend to negate suggestions that the numbers and/or clustering of secondaries destroy the effectiveness of crater counting as a chronometric tool.

1. Introduction

In recent years several authors challenged the ability of crater chronometry techniques to assess ages and evolution of the surface, at least in the case of using small impact craters [Chapman, 2004; McEwen and Bierhaus, 2006; McEwen et al., 2005; Robbins and Hynes, 2011a, 2011b; Daubar et al., 2013]. However, the small impact craters observed at high resolution on the Moon and Mars, if we understood their formation rates, would allow valuable measurements of surface ages and/or crater survival times (which in turn gives a measure of erosion/deposition rates) on small, localized formations. Thus, the understanding of small-crater formation is crucial. In this paper, we will first review some of the literature about secondary cratering and then present new data, derived from the young, 6.9 km impact Martian crater Gratteri and its secondary fields. We analyze the secondaries' morphology and distribution and discuss the uncertainties that secondaries may bring to assessment of ages and evolutionary processes from studies of impact crater size distributions.

2. Review of Secondary Cratering and Crater Count Techniques

Modern empirical discussion of secondary cratering began in 1964 with Ranger VII's impact on the Moon and its high-resolution imagery of the lunar surface. Here we review that history, because it played a role in the emergence of recent controversies on secondaries.

2.1. The Ranger Lunar Era

Ranger VII revealed for the first time the population of subtelescopic craters in the lunar mare—i.e., diameter $D < 2$ km. These small craters had a steeper-sloped size distribution than craters of $D > 2$ km, and their origin seemed puzzling at the time. In both systems of crater data plotting used here (log-differential plots and cumulative plots; Hartmann and Neukum [2001]), the slopes were about -3 to -4 , compared to a value closer to -1.8 for the craters of $D > 2$ km [Hartmann et al., 1981]. Authors suggested that many of these small craters are secondary impact craters, created by impacts of objects ejected from larger impact craters [Shoemaker, 1965; Shoemaker et al., 1970]. Shoemaker made counts of obvious secondaries around certain large lunar craters such as Copernicus, showing that this known “secondary” population had much steeper slope in

the size-frequency distribution (SFD) than the slope found among the larger primary craters. Therefore, Shoemaker's view was that most or nearly all of the small craters ($D < 2$ km) were secondaries. Secondaries close to fresh primaries and clustered in strings along rays were obvious, but those more distant and widely scattered, which we call field secondaries, were difficult to separate convincingly from small primaries. First reports on this issue found that the largest single Ss from the larger fresh lunar P craters ran up to about 5% of the size of the primary [Schultz and Singer, 1980; Hirata and Nakamura, 2006], indicating that basin secondaries might reach diameters of 20 km or more [Wilhelms, 1976; Hodges and Wilhelms, 1977]. On Mars, the largest S from a given P are approximately 2% [Schultz and Singer, 1980; McEwen et al., 2005; Werner et al., 2009].

McEwen et al. [2005], after studying the secondary field around Martian crater Zunil, proposed scenarios in which much of the "total" steep branch (Ss + Ps), at the smallest sizes, is dominated by secondaries. Werner et al. [2009] concluded that the largest Ss from a given P impact can have a slope as steep as -5 but that the curve then rolls over to shallower slope at a smaller size ($< 70\%$ the size of the largest Secondary). Werner et al. thus proposed that at least parts of the steep sloped branch of the "total" steep branch curve on both the Moon and Mars could be dominated by primaries [Werner et al., 2009].

Questions about the Ss/(Ps + Ss) ratio thus go all the way back to the 1960s and when Hartmann [1966, 1967a] began studies of lunar and Martian crater size distributions; in order to derive chronometric information, he elected not to try to separate primaries from secondaries but to make counts of the total population of "field craters," i.e., the primaries and more or less randomly scattered field secondaries, excluding obvious localized clusters and rays. Admittedly, counts restricted to primaries should give clearer age information, but the prospect of identifying and throwing out large numbers of craters as secondaries, based on entirely uncertain criteria or personal assumptions, seemed more alarming than accepting the total of Ps + field Ss as a proxy for age. After all, secondaries must accumulate with primaries, and vice versa. When Apollo and Luna samples allowed dating of lunar landing sites, crater counts of the Ps + field Ss total from these sites showed a correlation of the radiometric ages, giving some confidence in the general technique [Hartmann, 1970, 1972; Neukum et al., 1975a, 1975b, Werner et al., 2009]. This established that the total densities of field craters, P + field S, excluding clusters and rays, does correlate with age. Hartmann discussed these issues in the first of a series of lunar crater count papers [i.e., Hartmann, 1967a] and explicitly described making counts of total numbers of P + field S instead of attempting to identify and count primaries alone. We thus believe that counts of P + field S give useful chronometric information but also that the system can be refined as information about the field S component improves.

2.2. The Mariner/Viking Era

When Mariner 4 returned the first high-resolution photos of Mars in 1965, the images showed that populations of visible multikilometer Martian craters typically had a shallower slope than the lunar crater production function [Öpik, 1964]. Öpik [1964, 1965] immediately explained this by suggesting that smaller Martian craters would likely have shorter survival times than big craters, just as they do on Earth. He commented, without proof, that gradual infill of Martian craters, for example by blowing dust, would make the slope shallower by unity (i.e., altering a slope of -2 to -1 .) Chapman et al. [1969] gave a derivation of this result, supported by Hartmann [1971]. Hartmann [1966] coined the term "crater retention age" to emphasize that craters do not necessarily measure the age of the underlying rock unit but rather the retention time, i.e., survival time, for craters of each given diameter and depth, on that surface. On lunar surfaces, the crater retention age may usually be the formation age of the geological unit, but on most Martian surfaces (as on Earth), this "Öpik effect," as we call it, implies that the smaller craters give younger ages than the larger craters. This fact has sometimes been presented as a weakness of the system [Plescia, 2005] but is actually a potential strength of the system, because it allows analysis of geological processes acting at different scales, for example, measurements of the erosion and deposition rates as a function of size and depth [Kite et al., 2013]. The rapid loss of small craters by such processes is, of course, entirely familiar on Earth.

2.3. The MGS Era and First Attempts to Extend the Production Curve to Small Diameter

Starting in 1997, Mars Global Surveyor allowed a sudden, revolutionary extension of the Martian crater SFD to $D \sim 10$ m [Malin et al., 1998; Malin et al., 1998; Hartmann et al., 1999] and an explosion of interest in how few-meter-scale Martian craters might be used to refine information on chronology and geological processes.

A reliable *production* function shape in the decameter range is highly desirable for studying age relationships and erosion/deposition effects on small (kilometer-scale) geological formations. Measuring the production function on either the Moon or Mars is very difficult, because the small craters go into saturation at $D \sim 200$ m on lunar mare surfaces of average age of about 3.4 Ga and are highly affected by erosion and deposition processes on Mars. Neukum and coworkers [Neukum and König, 1976; Neukum, 1983] attempted to extend the crater size frequency distribution (SFD) below $D \sim 300$ m by making counts on the interiors or ejecta blankets of young, large lunar craters such as Tycho and Copernicus and then combining the counts from various D intervals into one curve. Neukum and Ivanov converted Neukum's lunar crater production SFD to Mars [Neukum and Ivanov, 1994; Ivanov, 2001]. Hartmann made independent conversions to Mars and published several iterations of his isochrons, with improvements based on incoming data. The most recent "2004 iteration" [Hartmann, 2005] used telescopic lunar crater catalog data scaled to Mars for craters of $D > \sim 2$ km, then adopted the Neukum and Ivanov shape at $D < \sim 500$ m but then further adjusted that curve shape at $D < \sim 20$ m for atmospheric breakup of Martian meteoroids as predicted by Popova *et al.* [2003].

A strength of such efforts is that Hartmann and Neukum/Ivanov worked more or less independently but obtained very similar results in terms of SFD shapes and crater production rates, as discussed in their 2001 joint review [Hartmann and Neukum, 2001; Neukum *et al.*, 2001; Ivanov, 2001]. Hartmann [2005] estimated that uncertainties in absolute ages could be a factor of 2 to 4; this is larger than Neukum estimated. Such uncertainties may seem outrageously large to a terrestrial geologist, but when one considers that on Mars we are trying to distinguish among ages of 10^5 , 10^6 , 10^7 , 10^8 , and even 4×10^9 years, factors of 2 to 4 are gratifyingly small.

2.4. Modern Studies of Martian Small Crater, and Controversy About Secondaries

The discovery of widespread secondary population on Europa [Bierhaus *et al.*, 2005] and of the widespread system of secondary craters around the 10 km primary Martian crater Zunil by McEwen *et al.* [2005] led to assertions in both papers that crater chronometry may give false results because of problems with secondaries. McEwen *et al.* [2005] suggested that crater chronometry on Mars may be off by factors of as much as 700 to 2000, assuming that the crater counters were trying to count and plot only primaries. However, the assumption was wrong, since counters count the total of primaries and accumulated field secondaries, and the isochron plots represent that total.

The Zunil studies posited enormous secondary population and implied that a Martian value for (field S)/(P + field S) is around 0.999 at decameter sizes [McEwen and Bierhaus, 2006; McEwen *et al.*, 2005]. The actual detection of small primary impact craters forming on Mars, from Mars Global Surveyor data [Malin *et al.*, 2006] revealed the current crater production rate for ~ 10 – 20 m primary craters, and according to several early analyses this rate fell below the Hartmann and Neukum production curves by a factor 2 or less [Hartmann, 2007; Ivanov *et al.*, 2009; Quantin *et al.*, 2007], rather than being some around 10^3 times lower, as implied by McEwen *et al.* [2005]. Additional detections of primaries at rates perhaps 4 to 8 times lower than the estimate of P + field S from Hartmann and Neukum [2001] have been made by Mars Reconnaissance Orbiter [Daubar *et al.*, 2013; Daubar *et al.*, 2014]. One way to interpret these observations is that they allow for a substantial fraction of field secondaries in the P + field S counts, perhaps 1/2 to 7/8.

On the positive side, vis-a-vis reliability of the crater chronology using small-scale impact craters, our group showed that the published isochrons pass an interesting test proposed by McEwen *et al.* [2005]: compare the expected formation interval of craters of a given size to the crater retention age for the small-scale crater population that postdate the crater formation. Hartmann *et al.* [2010] did this test for Martian rayed craters that are supposed to be the youngest craters in their size range on Mars, and in every case the authors found the predicted population of craters, giving ages near, or a few times, the expected formation ages.

Robbins and Hynek [2011a] continued the debate by presenting 24 Martian primary craters from 19 to 222 km in diameter and then plotting secondary fields around them. Their study gives useful data on the characteristics of the secondary crater systems, and they conclude that contamination by secondaries is widespread (i.e., that secondaries may be present everywhere), arguing that 30 Holden-sized (153 km) events would contaminate the crater population $D < 5$ km across the entire planet. If this conclusion is right, then the term "contamination" is not appropriate because crater counters are deliberately counting a mixture of both primary and secondary craters and the crater chronology has been defined with counts that include both populations. Hartmann [2007] pointed out that the new data suggest that at ~ 20 m, Ps dominate in the first

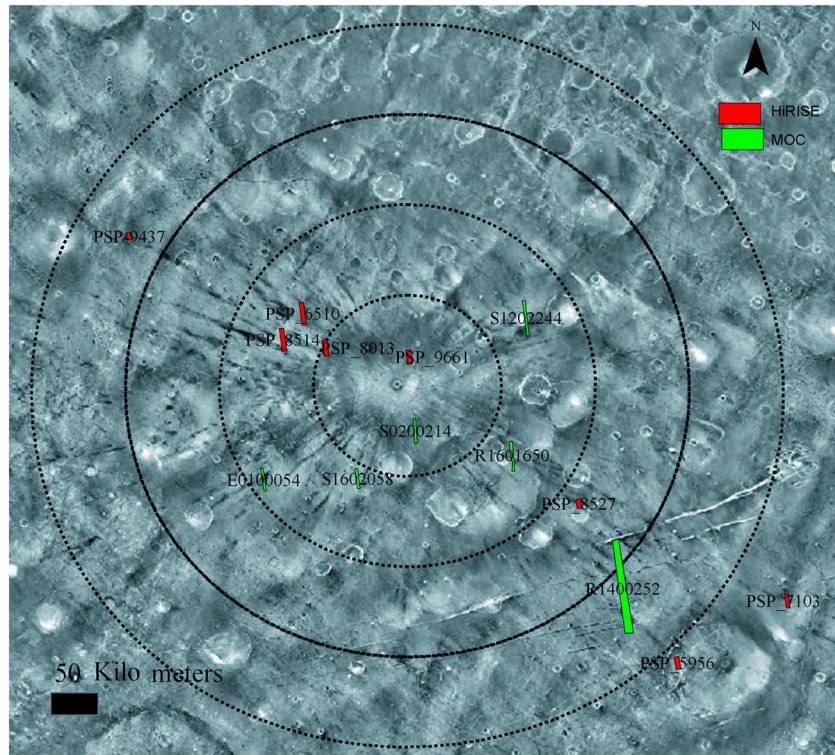


Figure 1. Gratteri crater context: Nighttime THEMIS infrared images illustrating the rays and the location of HiRISE (red squares) and MOC (green squares) images used in this study for crater counting. Circles around Gratteri are every 100 km. The ID of the images is given in Table 1.

~10⁶ years, but Ss could dominate after 10⁷ years. Our present paper attempts to delve into the problems associated with secondary ejecta on Mars and their effect on crater chronometry as it is actually practiced.

3. Gratteri Impact Crater

Gratteri crater, $D = 6.9$ km, is located in Memnonia fossae region at 17.7°S and 160.1°W (Figure 1). The crater is notable for its strong pattern of rays, revealed in Thermal Emission Imaging System Spectrometer (THEMIS) nighttime imagery (Figure 1) and suggesting that it should be one of the youngest craters in its size range [Tomabene *et al.*, 2006]. In this study, we combined the images (Table 1) at different scales using Geographic Information Systems (GIS) thanks to ArcGIS software. We map the rays and measure their area, for instance, or

Table 1. ID of High-Resolution Images Used in the Present Paper

Image ID	Distance From Gratteri (km)	Spatial Resolution (m/Pixel)	Camera
PSP_009661_1625	32	0.25	HiRISE
S0200214	45	4.44	MOC
PSP_008013_1630	103	0.25	HiRISE
s1602058	120	4.45	MOC
s1202244	144	4.5	MOC
PSP_006510_1635	145	0.25	HiRISE
R1601650	146	2.99	MOC
PSP_008514_1630	150	0.25	HiRISE
E0100054	192	4.24	MOC
PSP_008527_1600	230	0.25	HiRISE
R1400252	330	5.95	MOC
PSP_009437_1650	355	0.25	HiRISE
PSP_005956_1570	430	0.25	HiRISE
PSP_007103_1580	484	0.25	HiRISE

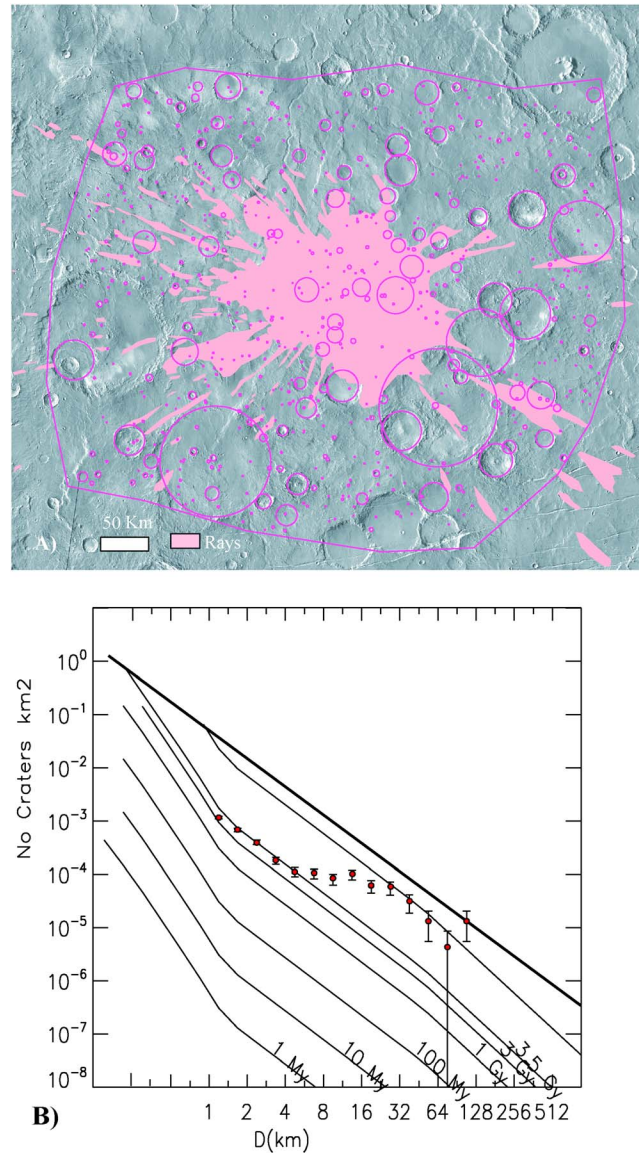


Figure 2. Crater populations of the background surrounding Gratteri. (a) Regional THEMIS daytime infrared mosaic around Gratteri, with various craters, counted by us, outlined in pink and dark infrared ray mapped in light pink. The counted area is also outlined in pink and is 241,100 km². North is at the top. (b) Log-incremental crater counts (showing numbers of craters in each diameter D bin) on isochron diagram in format developed by Hartmann. The data show that craters of $D > \sim 22$ km survive from Noachian time (approximately 4 Gyr ago) but that smaller craters ($D < \sim 4$ km to ~ 22 km) show a strong Öpik effect with lower survival times. Later diagrams will show similar effects at still smaller sizes.

fragmental and granular material down to the 400–700 m excavation depths, possibly bonded at depth with ice, and quite different from the probably intact lava flows that make up the much younger Elysium plains where Zunil was formed [Hartmann and Neukum, 2001; Hartmann and Barlow, 2006]. The significant difference in target material may cause differences in secondary ejecta, according to impact modeling by Melosh [1984].

The reader might assume that because the pre-Gratteri background is Noachian, it would be very heavily cratered or saturated with craters, and thus the Gratteri secondaries might simply be lost among the background

map the impact craters to measure their diameter and density, with respect to the distance from the well-identified primary crater. In our earlier study of the McEwen et al. test for young ray craters, we counted craters of $4 \text{ m} < D < 45 \text{ m}$ on a smooth floor deposit inside Gratteri, arguing that the crater must be at least as old as the deposit [Hartmann et al., 2010]. We obtained a crater retention age range of about 1 Myr to 20 Myr. We estimated that craters in the size range of Gratteri (5.5 to 8 km, in our binning system) have a formation interval of about 0.8 Myr. From these data we concluded that Gratteri is probably not the youngest crater in its size range but is one of the youngest, as expected for a crater showing a ray system. Such ray systems appear to last only some millions of years, on Mars, because the infrared signatures and even some of the shallow secondary craters are lost due to erosion and deposition effects (as would happen at an even faster rate on Earth).

Gratteri is located in an old cratered area, mapped as Noachian ridged plain (Figure 2a). The plain has been described as resembling similar Hesperian low-viscosity lava plains [Tanaka et al., 2014], and the ridges are described as “due to normal faulting but others may be volcanic constructs or compressional features” [Tanaka et al., 2014]. This is the type area for the Noachian ridged plains. Immediately adjacent (only a few Gratteri crater diameters away to the southeast) are old cratered highlands mapped as a Noachian cratered unit, interpreted as “materials formed during period of high impact flux; probably a mixture of lava flows, pyroclastic material, and impact breccia” [Tanaka et al., 2014]. If this material dates back to the Noachian intense-impact period (prior to ~ 3.7 Gyr ago) it may be mostly

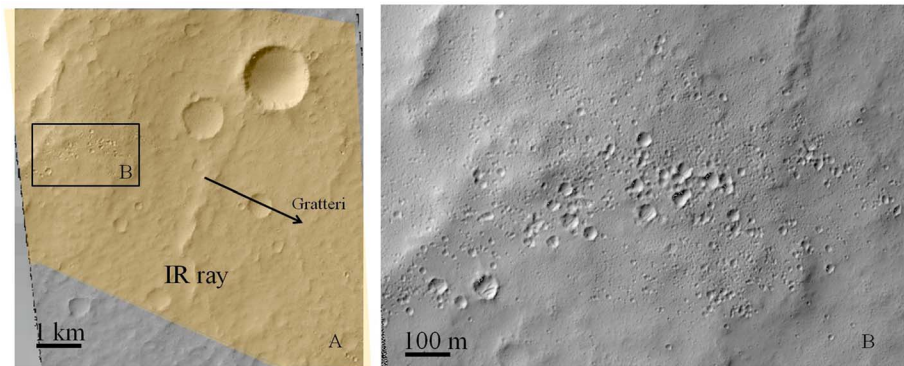


Figure 3. A portion of the Gratteri ray system ~100 km from Gratteri. (a) The region of infrared anomaly defining a broad ray segment. Gratteri direction is indicated as well as the location of Figure 3b close-up. The shaded yellow area corresponds to the ray mapped at larger scale on THEMIS nighttime images. (b) Example of one of many clusters scattered along the ray. (HiRISE image PSP_008013_1630.) North is at the top.

older craters. It is very important to note that, as shown in Figure 2b, this is not the case. Because of the Öpik effect, just as on Earth, erosion and deposition processes mean that crater survival times at 20–200 m scales are much less than the age of the planet and its surface, and the background small-crater densities are in fact quite low, as we discuss further in later sections.

As indicated in Figure 2, we made a regional count of the largest craters on THEMIS IR mosaic at 200 m of spatial resolution in a rectangular area stretching 520 × 450 km, centered on Gratteri itself. Striking information about the geologic history of the area emerges from this sort of plot. As is typical of all the oldest cratered highlands of Mars, the crater density of the very largest craters ($D = 32$ to 45 km) fall near the saturation line, indicating a Noachian age for the upper kilometers of crust and showing that the total cumulative effects of Martian erosion, deposition, and tectonics since have been inadequate to remove such large-scale topography since Noachian time. Also typical of the oldest cratered highlands of Mars, the interray craters of $\sim 4 \text{ km} < D < 32 \text{ km}$ show a flattened segment where the SFD has much lower slope than the production isochrons, meaning that smaller topography has been lost by long, gradual processes, the Öpik effect. Craters in this size range tend to be degraded, many being shallow and partly filled with smooth deposits. As mentioned in the opening section, a vigorous literature, associated with the earliest Mars missions, documented how gradual processes such as infill can produce the flattened SFD [Öpik, 1965, 1966; Hartmann, 1966, 1971; Chapman, 1968; Chapman et al., 1969; Chapman, 1974; Jones, 1974; Chapman and Jones, 1977].

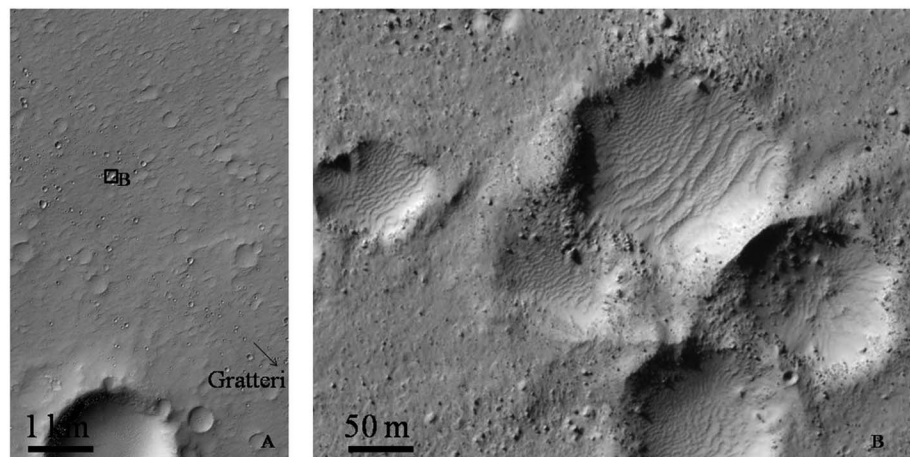


Figure 4. (a) HiRISE picture PSP_008514_1630 featuring an IR ray 150 km north west of Gratteri. (b) Close-up within a cluster. North is at the top.

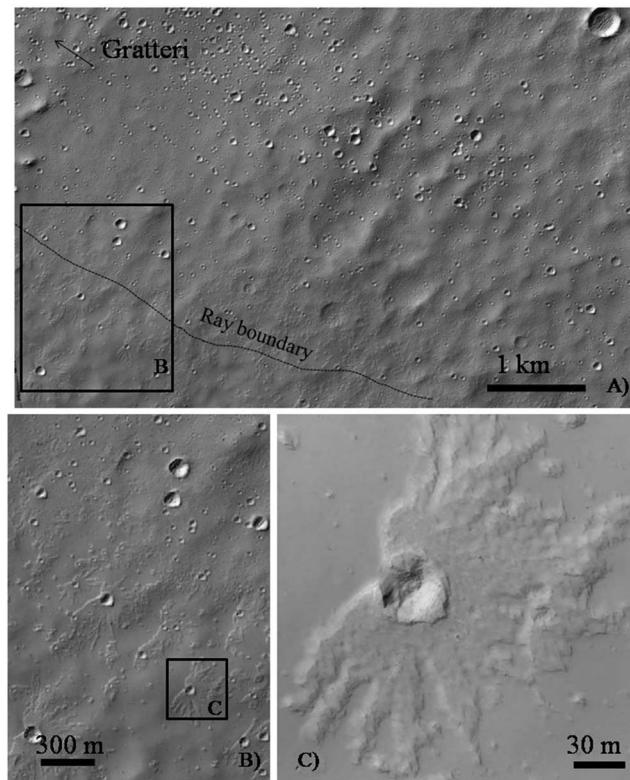


Figure 5. Rampart secondaries near the edge of rays (PSP_008527_1600). (a) Context of the boundary of a ray delimited by the dark line. Gratteri direction is indicated as well as the location of Figure 5b close-up. (b) Close-up on the boundary of an IR ray. The rampart secondaries are dense. Close-up Figure 5c is located. (c) Close-up on the rampart secondary indicated in Figure 5b. North is at the top.

At diameters of 4 km down to about 1 km (Figure 2), the data fall in the Hesperian time period, roughly around model ages 3 to 3.5 Gyr ago, by our estimate [Hartmann and Neukum, 2001; Hartmann, 2005]. The fact that the production isochron shape has been preserved from 4 km down to 1 km (or even ~250 m) suggests that medium-sized topography in that diameter range (original vertical depth $d \sim 1300$ m down to as little as 80 m) has been preserved in this area since Hesperian time. Hartmann and Neukum [2001] used this sort of quantitative, crater SFD-based reasoning to show that nearly all forms of obliteration processes (deposition, volcanism, fluvial activity, etc) decreased by 1–2 orders of magnitude around the end of Noachian time. As shown in later diagrams, we find evidence of additional small-scale obliteration effects operating at scales < 250 m km in this area, and we estimate that the smallest craters preserved since the Hesperian are about 250 m to 1 km across. In summary, Gratteri was emplaced 1–20 Myr ago on a Noachian plain that had a complex history of early erosional and depositional processes which reshaped the landscape at kilometer scales from Noachian through Hesperian times.

4. Study of the Gratteri Secondaries

4.1. Identification of Gratteri Secondaries

We failed to identify secondary craters on THEMIS images in the visible spectral range (18 m per pixel). This is because the THEMIS VIS frames do not have enough resolution to show most of the secondaries, which are mostly in size bins with $D \sim 16$ –45 m. The largest Gratteri secondaries we have noticed (identified by being the largest sharp-rimmed craters in clusters of sharp-rimmed craters inside the Gratteri rays) are around $D \sim 130$ m (see Figures 3 and 4). This is 1.8% of the size of the primary, Gratteri, itself. This is about half the value reported in Schultz and Singer [1980] and in Hirata and Nakamura [2006] for lunar impact craters, which is about 5%. It agrees, however, with reports about largest secondaries of Martian craters like Zunil, giving results around 2% [Schultz and Singer, 1980; McEwen et al., 2005; Werner et al., 2009].

Thus, study of the Gratteri secondaries requires Mars Orbiter Camera (MOC) images and High Resolution Imaging Science Experiment (HiRISE) frames. On these frames, the dramatic *infrared* ray structure is not visible, but the rays themselves are easy to distinguish as alignments of densely packed craters, some oddly shaped and prominent clusters of craters. Here we are interested in the relation of secondaries to crater counting, and we note that the rays are unlikely to go unrecognized or be missed by an experienced crater counter, especially inside the distance of around 120–230 km from Gratteri (roughly 18–33 crater diameter), where crater densities inside the rays are maximized. And, as we will discuss, beyond that distance the crater densities coinciding with areas of the “infrared rays,” as well as between them, appear to drop to lower values.

The secondary craters themselves are distinguished by several characteristics. First, one notes strong clusters of small ($D < 125$ m), sharp-rimmed craters spaced along the infrared rays (Figures 3 and 4). Second, the

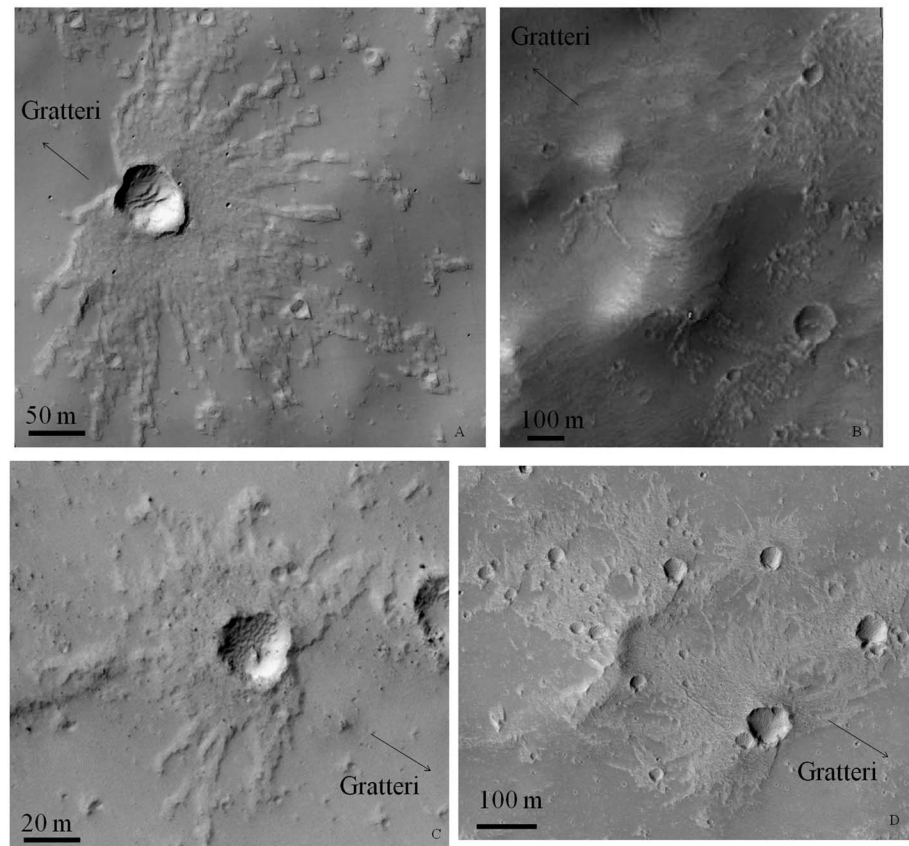


Figure 6. Rampart secondary, with direction to Gratteri marked by arrows. (a) Part of HiRISE image PSP_008527_1600. (b) Part of MOC image R1601650. (c) Part of HiRISE image PSP_008514_1630. (d) Part of HiRISE image PSP_006510_1635. North is at the top.

craters in those clusters reveal the morphology typical of the individual Gratteri secondaries strung along the rays in this region, namely small, sharp-rimmed, or somewhat deformed craters, mostly in size bins $D = 16$ to 65 m. Between the Gratteri rays, no such clusters of fresh-looking craters are observed. Scattered “field secondaries” are likely to exist between the rays, but they are not obviously recognizable. That is why we perform all our crater counts on the entire crater population, rather than trying to pick which small craters are primaries and then throw out the others.

4.2. Rampart Secondaries

At MOC resolutions (few meters), the Gratteri secondaries in the rays in most areas appear as relatively ordinary, small, impact craters, but in our set of HiRISE images we have discovered some fields along ray edges and outside rays where a nonnegligible fraction of these craters have a hitherto unknown morphology for craters at this scale. They are surrounded on most sizes by raised, star-shaped, or ray-like ejecta patterns that extend a few crater diameters, often strikingly absent on the side facing Gratteri. In other words, craters associated with Gratteri rays often have rampart-like ejecta blankets primarily on the side away from Gratteri and at azimuth angles ranging up to 90° from the anti-Gratteri direction. Indeed, many suggest “forbidden zone” or “butterfly-like” patterns typical of low-angle impacts [Gault and Wedekind, 1978; Herrick and Hessen, 2006]. We have given these the name “rampart secondaries.” Examples are shown in Figures 5 and 6. These rampart secondaries were found only beyond 100 km and primarily at distances from 100 km to 300 km from Gratteri. Usually, the rampart secondaries appear in groups in a concentrated area, such as shown in Figure 5 (especially Figure 5b). The rampart secondaries are distributed almost entirely between the rays and possibly with some concentration along the edges of rays, but rarely on the central axis of rays. Inside the ray at 100 m scale (as seen in Figure 5b), it is common to see a smooth, rolling surface broken by clusters of circular craters with sharp rims. The absence of the rampart secondaries around the downrange

line from Gratteri suggests fairly high-angle impact, probably higher than 17° from the horizontal. Just outside that same ray, however (as seen in Figure 5c), we see “clots” of irregular raised material that turn out (upon examination) to be rampart ejecta blankets with “forbidden zone” or “butterfly” patterns, around craters of roughly 20–100 m diameter. The ejecta patterns of the latter indicates very low impact angles, likely below 12° – 17° , and the trend toward butterfly patterns could indicate angles around 7° – 12° from the horizontal [Gault and Wedekind, 1978; Herrick and Hessen, 2006]. Thus, there appear to be two distinct classes of secondaries around Gratteri: sharply defined circular craters formed at higher impact angles in rays and the butterfly-like rampart secondaries formed at grazing impact angles at the edge of rays. We leave open the possibility that other groups of secondaries—less easily recognizable—may exist as well, such as circular secondary craters, not in clusters, outside the rays. Outside of the clusters, but inside the rays, we cannot distinguish whether scattered sharp, circular, small craters are mostly randomly scattered fresh “Malin et al. primaries” or mostly sharp round secondaries.

Anderson et al. [2003] compared modeling of impacts at 90° and 30° from the horizontal, for impact velocity 1 km/s, in the range for secondary craters. They found that the 30° impact has a strongly asymmetric velocity field in the first 5 to 10 ms, with highest downrange velocities and no material ejected under the flight path (back toward the primary crater). The material traveling at slowest velocity is symmetric and is what builds the rim adjacent to the crater. This modeling supports the idea of butterfly-like bilaterally symmetric ejecta fields on secondary craters at low angles and appropriate impact velocities.

If we compare a swarm of low-angle “butterfly rampart” forming projectiles impacting at $\sim 12^\circ$ – 17° with high-angle impact crater clusters, impacting at $\sim 45^\circ$, we can compare the impact velocities (assumed to equal the launch velocities; for this simple estimate we neglect atmospheric deceleration). The low-angle ejecta would have to be launched at higher speed to reach the same distance. For a low impact angle α velocity ratio is

$$V_{\text{at } \alpha} / V_{\text{at } 45^\circ} = 1 / \sqrt{(\sin 2\alpha)} \quad (1)$$

At a launch and secondary impact angle of 17° , an impact that would create the observed uprange forbidden zone in the rampart crater would have to move 1.3 times faster than the 45° “curtain” ejecta. At launch and impact angle 7° the ejecta would have to move 2.0 times faster. To date, we have found few, if any, transitional forms, and this suggests distinct phenomena during at least some impacts: a high-velocity, low-angle and a lower velocity, more conventional 45° ejecta curtain. One could assume that in the center of the ray secondaries are so densely packed that their ejecta overlaps, and these distinctive forms are masked. But it is not the case as there still are isolated secondaries, and no transitional forms are observed.

The cause of the rampart-like ejecta, with distinct thickness and a sharply defined leading edge, remains uncertain. Herrick and Hessen [2006, Figure 9] illustrate a similar, 280 m butterfly crater in the context of primary impact craters and comment that it “is much too small to have ramparts in the ejecta, presumably implying that mud flows (such as suggested for large Martian rampart craters, formed by impact into ice-rich material) are unlikely at this scale.” We note, however, that the general splotchy planform and texture of the thick ejecta are remarkably like those attributed to the classic, larger Martian rampart craters. Roughly similar asymmetric patterns exist among Zunil secondaries [Calef et al., 2009], but their ejecta blankets seem not as thick or rampart-like as the Gratteri butterfly rampart secondaries. The difference might relate to ice being more abundant in the upper few meters of the fragmental ancient regolith target material at Gratteri than in the upper few meters of young lava flows at of the Elysium plain around the Zunil impact site, but no direct or indirect evidence supports this hypothesis. The fragmental material, with its increased pore space, may be more easily recharged with ice during climatic variations associated with obliquity changes [Forget et al., 2006]. Thus, the rampart craters of Gratteri may plausibly involve butterfly pattern ejection of muddy slurry from the low-angle impacts into material with shallow ice.

Recently, a mechanism for the production of crater rays was proposed [Shuvalov, 2012], which is based on the interaction of primary impact-induced shock waves with nonuniformities of the target surface (target relief). This interaction results in the formation of an ejecta jet, which produces a ray-like nonuniformity in the deposit distribution. Another idea is that the field secondaries between the rays impact at a time such as to interact with the ray-forming ejecta jet from Gratteri. The ray-forming ejecta jet could include secondary craters producing fragments of different sizes as well as entrained vapor/atmosphere/dust. This jet is some kind of flow which might pile ejecta from secondaries in the downrange direction [Shuvalov, 2012]. Close to Gratteri, the boulders from primary would be fast enough to begin to make craters (as opposed to boulders

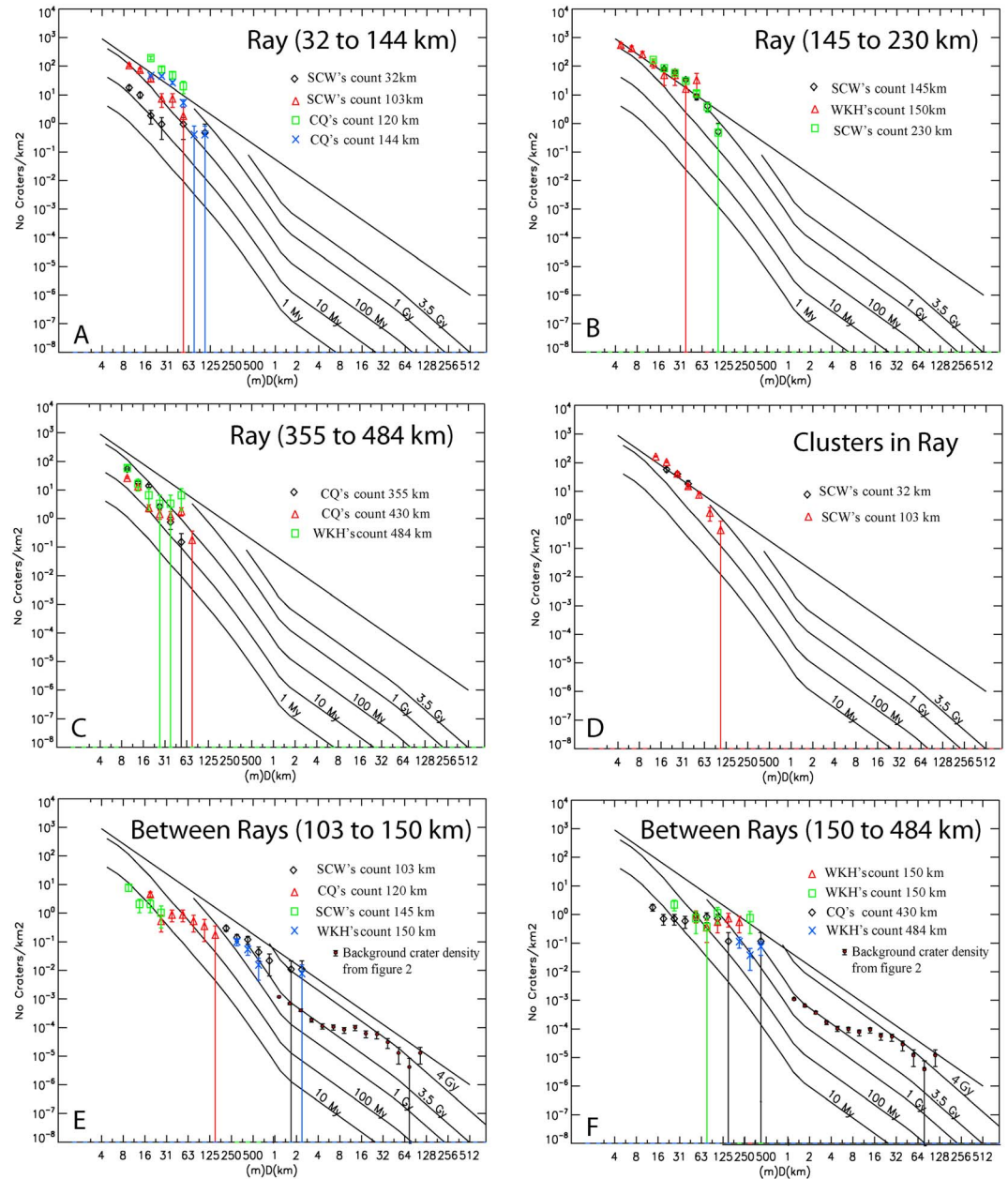


Figure 7. Crater size distribution at various distances from Gratteri inside and outside the rays. WKH denotes counts performed by W.K. Hartmann, SCW by S.C. Werner, and C.Q. by C. Quantin. (a) Crater counts performed from 32 km to 144 km inside the rays. (b) Crater counts performed inside the rays from 145 km to 250 km. (c) Crater counts performed inside the rays from 355 km to 484 km. (d) Crater counts performed inside clusters in rays. (e) Crater counts performed outside the rays from 120 km to 145 km. (f) Crater counts performed outside the rays from 150 km to 420 km. In both Figures 7e and 7f, crater count done at low resolution on the plain surrounding Gratteri presented in Figure 2 are plotted to be compared to crater densities outside the rays. Note that the isochrones are plotted just as benchmarks not to attribute ages from the plotted crater counts. These plots are incremental diagram where the size bin is $\sqrt{2}$. We assume a Poissonian error and use \sqrt{N} as error bar. We are not representing the crater count down to the diameter class with the highest number of craters. This threshold is determined by the image resolution and is different from a count to another. The counted areas of each individual count are in the Table S1 in the supporting information. Also, an example of crater mapping is shown in Figure S1 of supporting information.

landing intact) but impact too slow to produce much ejecta, which might explain deficiency of butterfly-like ejecta in that zone. At a middle zone, impact velocities would be higher, and jet interaction might pile ejecta from secondaries in the downrange direction. The larger the distance, the weaker the jet flow, and the jet effects might be too small to pile up downrange ejecta.

Still another hypothesis about rampart secondaries is that the ray emplacement process itself might be involved. We see evidence within the rays that there is some piling up of fine materials (grains smaller than HiRISE resolution) during the ray production, so that the boulders making the crater clusters commonly seen along the rays impacted into loose material different than the surrounding background. We noted that intercrater surfaces within the ray have smooth appearances. *Schultz et al.* [2007] showed that a 30°-from-horizontal impact into three granular materials of varied porosity produced a circularly symmetric crater with sharp rim in low porosity material, but an ejecta pattern piled mostly downrange (away from Gratteri) in medium-porosity material. And high-porosity, low-density material produced craters with very poorly defined rims, with much fine material ejected (which in the case of Mars could be blown away).

In any case, Gratteri's "rampart secondaries" are an unusual category of Martian craters, which, when properly understood, may tell us something about (target-region-specific) ejection processes from Gratteri-sized primaries and/or tell us something about ejection of muddy slurries from low-angle impact secondaries (again in certain specific regions or during certain climatic episodes, where/when ice is present in the upper few meters of target material).

5. Crater Size Frequency Distributions in Regions Influenced by Gratteri

Our study area is a 400 km radius circle around Gratteri crater because Gratteri rays have been observed in this range of distance to Gratteri (Figure 2). Inside the study area, Gratteri's rays have been mapped on THEMIS nighttime IR images which served to define the classification inside versus outside the rays. In this area, we analyzed the crater size frequency distributions at various distances from Gratteri and in various contexts including inside various rays and between the rays. Our goal was to assess possible variation of the crater size frequency distribution (craters/km² and shape of the size frequency distribution curve), according to the radial distance from the primary impact crater Gratteri and also azimuthal transects from outside to inside of rays. Note here that the spatial resolution of the image affects the range of crater diameter mapped. We consider that from about 8 pixels, we can detect all the craters on an image, but it is dependent also on the quality of the image. We can count down to 6 pixels on some high-quality images on young terrains with sharp-rimmed, well-defined craters, while on other images the threshold is at 10 pixels. For crater mapping on HiRISE, for instance, there should be no resolution effect until crater smaller than 2 m. Note also that image coverage is not equal in all directions from Gratteri, leading to possible observational bias if there are asymmetries in the ejecta distribution (not obvious from the THEMIS infrared images).

5.1. Crater Size Frequency Distribution at Various Distances From Gratteri

The size-frequency distributions (SFD) observed inside the rays are shown in Figures 7a–7d, while the observed crater SFDs between the rays are reported in Figures 7e and 7f. In this section, we focus our study on the SFD for impact craters smaller than 125 m to address the issue of small impact crater contamination due to secondary craters.

Inside the rays, the SFD observed at 32 km from Gratteri follows the slope of the isochrons, around the 10 Myr isochron (Figure 7a). Here and later in this paper, our references to isochrons, especially inside the rays, are often intended only to examine the *shape* of the measured crater SFD, relative to our estimated isochron shape of the production function of primaries + field secondaries, averaged in time. We can of course not measure a surface age from crater counts inside a ray, since the surface probably got saturated with small craters in a few-minute event. What interests us inside rays is the extent to which the secondaries in the ray have the same SFD shape as the postulated Martian isochron SFD for primaries + field secondaries. In other words, do secondaries at decameter scale have the same size frequency distribution as primaries (which, after all, are mostly "asteroidal secondaries" from collisions between or on asteroids) ?

Farther away, at about 100 km from Gratteri (as also seen in Figure 7a), the crater density is 1 order of magnitude higher than at 32 km, i.e., following the 100 Myr isochron. Between 120 and 145 km from Gratteri, our counts suggest that the crater density inside the rays is above the saturation curve, and another 1 order of

magnitude higher than the density at 100 km (Figure 7a). Note that the position of the saturation curve depends on the cratering over the entire SFD. If craters form in a limited area (as with a cluster of secondary debris in a ray), then within that area the local crater density can easily rise above the saturation line, in a limited D range, and the SFD slopes may depart from the norm. Here the slope of the SFD appears smaller than the isochrons and is consistent with the saturation slope. From 145 km to 230 km (Figure 7b), we observe a similar trend suggesting that the SFD is lying near the saturation curve with the same slope as the saturation. At this distance from Gratteri, we observe the highest crater density of the whole area, and it is possible that even more impacts occurred but with some craters having been erased by saturation overlap effects (Figure 7c). From 355 to 484 km from Gratteri, the crater density is back down to the level observed at 32 to 100 km from Gratteri, lying between the isochrons 10 and 100 Myr. The slope of the SFD of our crater count is similar to the isochron slopes. If now we look at the SFD of a single cluster inside the rays (Figure 7d), we observe that the slope may be slightly steeper than the isochrons and is not inconsistent with result found by *Popova et al.* [2007] in their study of much larger clusters caused by large-crater secondary debris.

Between the rays (Figures 7e and 7f), both crater density and the SFD behave differently than inside the rays. From 120 to 430 km to Gratteri, the SFDs apparently have flatter slope than the isochrons. Such flat slopes are typical of old Noachian plains (i.e., pre-Gratteri background), which, in turn, is typical of the Āpik effect, expressing erosional or depositional processes that cause preferential loss of smaller craters. This may suggest that those areas are not dominated by secondaries, which have a steeper size distribution. As with craters inside rays, we observe an increase of the crater density outside the rays at about 150 km but by a somewhat smaller factor than inside the rays. This increase, at the same distance, suggests that at least some of the craters outside the rays are Gratteri secondaries, even if they do not dominate the population and are not easily identifiable. The flat distributions are comparable to the slope of background crater SFD observed at large scale and presented in Figure 2b, where craters of $D > 16$ km date back to Noachian times, and where craters at $D = 1\text{--}6$ km survive since Hesperian era. We find it difficult to identify individual secondaries between the rays, except for the rampart secondaries, and as noted above we suggest that there are fewer secondary clusters than around Zunil. We thus find it difficult to measure an exact crater density for Gratteri secondaries outside rays, since they are scattered among a dense and dominating population of pre-Gratteri craters. To go further, we now focus on the relationship of crater density with the distance to Gratteri both inside and between the rays.

In Figures 8a and 8b, we show the crater density according to the distance to the primary Gratteri for diameter bins between 8 m and 62 m in diameter. Even if the results show a large dispersion of the crater density at same distance (sometimes as large as 1 order of magnitude), some trends emerge. This reveals that crater density both inside and outside the rays displays a maximum between 100 and 250 km from Gratteri. The crater density in the range between 100 and 250 km is around 5 times higher than that at 450 km for crater both inside and outside the rays. We note also that the crater density inside the rays exceeds some 30–40 times the number outside the rays. We also compare the dependence on distance and with respect to the size of the craters. Inside and outside the rays, the smaller the diameter is, the more the crater density is increased between 100 and 200 km from Gratteri and most prominently at a distance of about 20 times the Gratteri diameter. The density for the diameter bin between 43 and 62 m seems to be the less affected size bin, while the density for diameter bin between 8 and 11 m is the most affected size bin. To further compare the variation inside and outside the ray, Figure 8c focuses on the crater density at sizes between 11 and 16 m in diameter according to the distance to Gratteri inside and outside the rays. This reveals that the crater density outside the rays shows a slight increase at 150 km, while the crater density inside the rays is strongly affected with an increase by a factor of more than 100 times the density at 30 km. These results suggest constraints on the ejection mechanism forming secondary craters during the Gratteri impact, indicating a maximum of secondaries around 20 times the Gratteri diameter from Gratteri, both in and outside the rays. The dynamic implications of this process are analyzed in section 6. Our results also suggest that secondaries are concentrated inside the ray where the crater density may reach values 40 times the density outside the rays, while the densities are so much lower outside the rays that at most distances they seem to be near or in the noise level.

5.2. Crater Density Transect at 150 km From Gratteri

To go further, we made crater counts along a ray crosscutting transect, at HiRISE image scale. HiRISE image PSP 008514_1630 offers a 25 km long transect that crosses two rays, about 150 km from Gratteri, near the

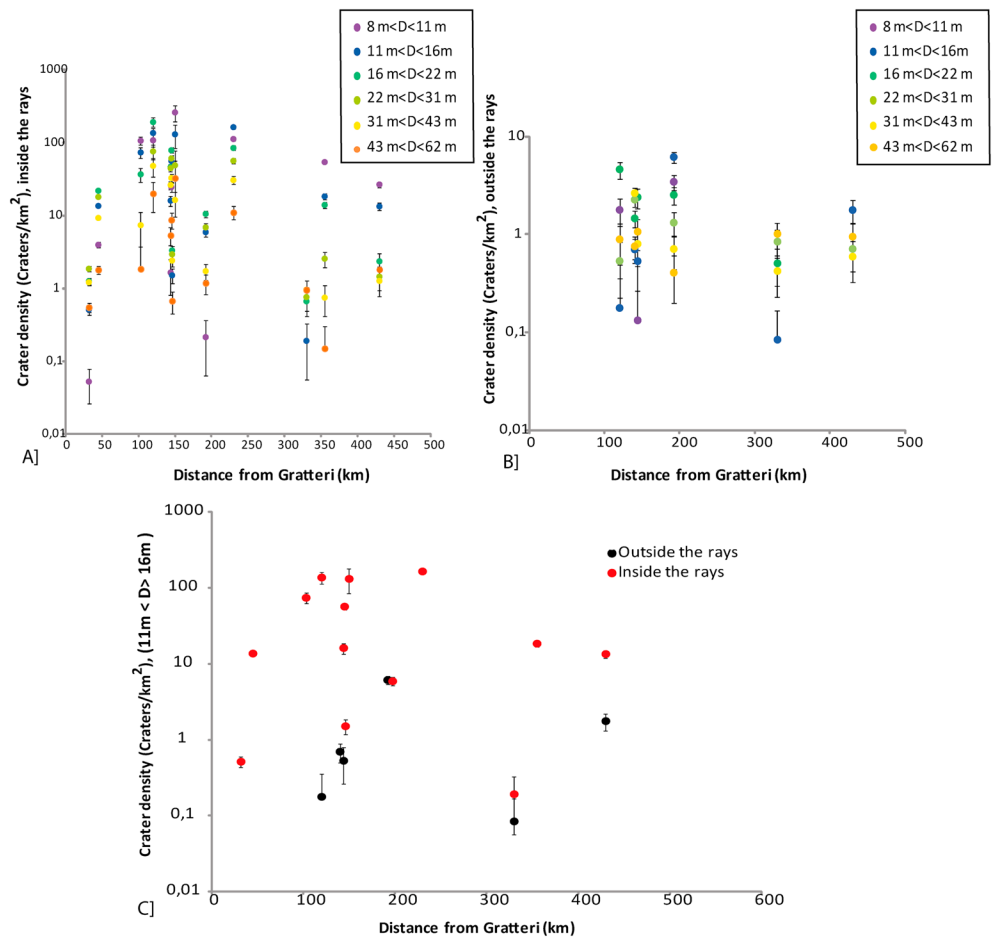


Figure 8. Crater density versus the distance to Gratteri: (a) Density of craters at various diameters $D = 8$ m to 62 m according to the distance to Gratteri in kilometers inside the rays. (b) Density of craters at various diameter $D = 8$ m to 62 m according to the distance to Gratteri in kilometers outside the rays. (c) Density of impact crater from 11 to 16 m of diameter according to the distance to Gratteri. Black circles denote crater density outside the rays, while red circles denote crater density inside the rays.

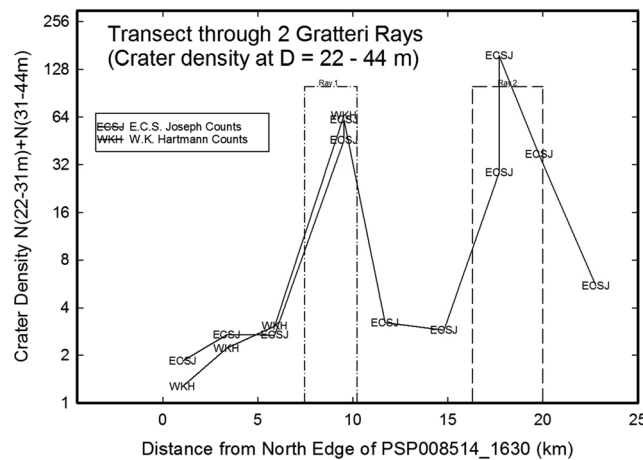


Figure 9. Plot of N (number of craters) at 150 km from Gratteri for impact craters from $D = 22$ m to 44 m in 10 similar size boxes along a 25 km transect crossing perpendicular two rays and interrays areas. ECSJ denotes E.C.S. Joseph counts, and WKH denotes W.K. Hartmann counts.

maximum secondary crater density inside the ray. The transect is cutting the rays almost perpendicular to the ray direction. This offered a chance to examine crater densities along a transect as one travels north to south across areas between rays but crossing two rays. It tests directly the consequence if a crater counter failed to recognize that a ray was present. Ten smaller areas of equal size were mapped separately from north to south along the transect. Figure 9 shows the number of craters inside the different areas along this transect on a logarithmic scale of crater density. Crater density differences inside and outside the rays are striking. We noted that the difference between crater SFDs inside and outside

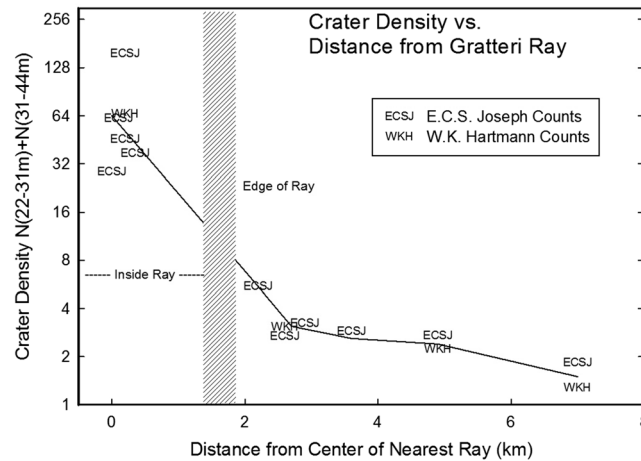


Figure 10. Plot of N (number of craters) at 150 km from Gratteri for impact craters from 22 m to 44 m in similar size boxes along a 8 km transect from the center of a ray, across its boundary, into the interray area. ECSJ denotes Emily Joseph counts, and WKH denotes W.K. Hartmann counts.

of rays is especially strong at crater diameters $D \sim 16$ m to 44 m, and as a parameter to represent crater density, we chose the sum of crater densities in two D bins, 22–31 m and 31–44 m, consistent with section 5.1. We see that the crater densities rise from ~ 1.5 craters/ km^2 in these two bins to about 50 or 100 craters/ km^2 . In other words, crater densities inside the rays, at this 150 km distance from Gratteri, are of the order 30 to 70 times the densities between the rays. The areas inside the rays are intensely pocked with scattered small craters with various degrees of clustering. The areas between the rays are much less cratered but presumably have a mixture of primaries, some Gratteri secondaries, and other “field secondaries.” In Figure 10, we plot the

same crater density data as a function of distance from the central axis of the nearest ray. This plot emphasizes how the crater densities may rise slightly as we approach a ray (from about 1.5 to as much as three or five craters/ km^2 in the two D bins mentioned above) but jump dramatically to values of 60 inside the ray.

5.3. Ratio of Secondary in Rays and Outside the Rays

It seems that secondaries impact craters located inside the rays are easily recognizable because they are clustered. As we have mentioned, our practice in chronometric crater counting is simply to exclude areas containing such clusters and ray alignments of craters from our counts, whether a parent primary crater is recognized or not. Compared to fresh primary clusters [Daubar *et al.*, 2013], crater clusters suspected to be secondaries are less densely packed with craters and are elongated compared to the primary ones from current era. A fragmenting meteoroid in Mars atmosphere ejects fragments at some uncertain, modest lateral (sideways) velocity, but they have only some seconds to spread out laterally [Popova *et al.*, 2003, 2007]. Thus, most primary clusters can have widths of a few hundred meters. But secondaries eject fragments during ejection, ascend through the atmosphere, may have minutes of flight time up and back down, and so spread over larger distances. Widths of rays and some clusters of 500 m wide secondaries are typically more like 4–6 km. But by deleting not only questionable clusters but also the area of those clusters from the counts, we restrict our existing counts to scattered primaries and field secondaries and side-step the issues of clusters.

The main issue for us here is to understand the fraction of secondaries that are inside the rays and clustered away from the “field secondaries,” which are outside the ray, semirandomly distributed. The surface covered by rays around Gratteri is $1.6 \times 10^4 \text{ km}^2$. The whole surface included into a circle of 450 km radius (the distance of the farthest observation from Gratteri we present here) around Gratteri primary crater is an area of $6.4 \times 10^5 \text{ km}^2$. The surface with rays is thus about 2% of the 450 km radius circle around Gratteri.

Crater density inside and outside the rays at various distances are used to estimate the fraction of the secondaries in the rays and outside the rays. That conclusion is based on the results presented in Figure 8 to assess the ratio of impact inside the rays and impacts outside the rays at various distance ranges from Gratteri (Table 2) and consider the most populated diameter bins 15–32 m (at least in order of magnitude). We assume here that the background number of craters predating Gratteri secondaries is the crater density invariant with distance. We also have to keep in mind that that the results of Figure 8 have a certain scatter, so the following approach should be considered more as an estimate than as a precise result. First, if we assume that the ray area holds the same fraction of total area at any distance (i.e., the rays area is increasing as square distance), corresponding values are given in the fourth column of Table 2. The fraction of craters in the ray is decreasing with distance, and total number of craters approaches the background number. Second,

Table 2. Calculation of Gratteri Secondaries Inside Rays and Outside Rays

Distance From Gratteri	Mean Crater Density N_{in} , Craters/km ² (Figure 8, $D \sim 15\text{--}32$ m)	Mean Crater Density N_{out} , Craters/km ² (Figure 8, $D \sim 15\text{--}32$ m)	Fraction of Secondaries Inside According to the Hypothesis That Ray Area Holds the Same Fraction of Total Area at Any Distance	Fraction of Secondaries Inside the Rays According to the Hypothesis That the Width of the Ray Is Approximately Constant at Any Distance From Gratteri
0–80	28.6	----		
80–200	155.5	5.6	42%	57%
200–300	164.6	10	30%	30%
300–400	18.2	1.4	25%	19%
400–500	17.2	3.1	12%	7%

if we assume that the width of the ray is approximately constant at any distance from Gratteri (fifth column), the fraction of craters in the ray is decreasing faster as the relative ray area is decreasing.

It appears that on average about 30% of the secondaries are concentrated in the rays based on this simple calculation. That means that about one third of the secondaries are concentrated in clusters in about 2% of the surface around Gratteri. It also means that the remaining 70% of secondaries are scattered on 98% of the rest of the surface.

These numbers have consequences for understanding the distribution of secondary craters and their effects on crater counts as discussed below in the section 7. The crater count systems developed by Hartmann and independently by Neukum avoid areas of rays and obvious clusters and attempt, instead, to count the total of primaries and semirandomly scattered “field secondaries” (outside rays) as a proxy for crater retention ages [Hartmann and Neukum, 2001]. Similarly, near-field secondaries in the range of up to about 10 primary crater radii have been described by numerous publications, which can be excluded easily because they are part of an obvious field around a large, fresh primary.

5.4. Comparison With Zunil Analysis

McEwen *et al.* [2005] emphasized large numbers of secondaries around the young Martian ray crater Zunil ($D = 10$ km, relative to 7 km for Gratteri) and reported hydrodynamical simulations of the production of secondaries,

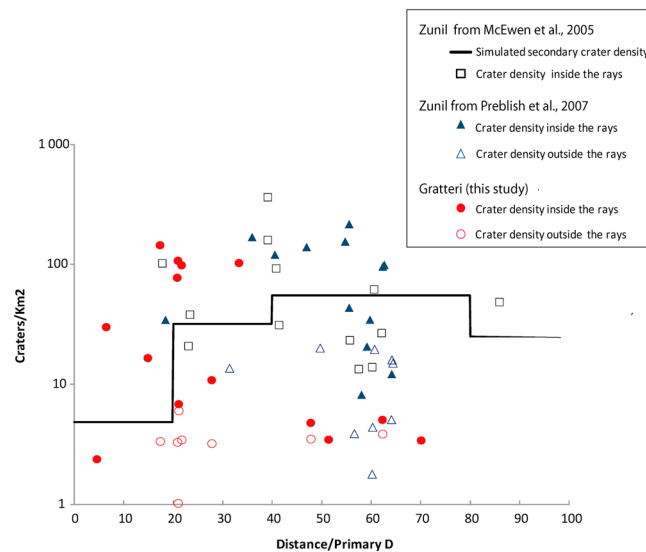


Figure 11. Comparison of crater density around both primary craters Zunil and Gratteri. The raw data from McEwen *et al.* [2005] are crater density $D > 10$ m. To convert crater density $D > 10$ m to $D > 15$ m like the data from Preblich *et al.* [2007] and data from our study, we divide the $D > 10$ m density by 2 because that is the average ratio between the crater density $D > 10$ m versus crater density $D > 15$ m.

predicting secondary crater numbers as a function of distance to Zunil. They predict a maximum of secondaries for an impact the size of Zunil between 400 and 800 km (Figure 11). From measurements of crater density inside the rays, the same authors report a maximum of crater density at 400 km of Zunil ($\sim 40D_{primary}$) (Figure 11). This distance is about double what we observe for Gratteri ($\sim 20D_{primary}$). A follow-up paper by Preblich *et al.* [2007] reported crater counts done mainly around 600 km westward from Zunil ($\sim 60D_{primary}$). In Figure 11, the McEwen *et al.* [2005] and Preblich *et al.* [2007] data show that the crater density inside the rays at $60D_{primary}$ from Zunil is as high as (and also higher than) our measurements inside the rays at about $20D_{primary}$ from Gratteri. They found the crater density outside rays of Zunil at $60D_{primary}$ is about 6–10 times less than the density inside the rays, in agreement with what

we observe for Gratteri but at $20D_{\text{primary}}$ (Figure 11). But here we note that westward of Zunil, a newly recognized rayed crater, now named Corinto, produced rays of secondaries that crosscut the rays of Zunil in that same westward area. Some of the rays and secondaries mapped in *Preblich et al.* [2007] are not radial to Zunil, but belong to Corinto rays system as they do not match Zunil radial azimuth but the Corinto one. So the counts reported in *Preblich et al.* [2007] are a mixture between two secondary source craters: Zunil and Corinto, and thus too high for Zunil alone.

McEwen et al. [2005] included a hydrodynamical simulation of Zunil secondaries (black line in our Figure 11). The simulation done in *McEwen et al.* [2005] distributed the secondaries uniformly in azimuth, i.e., with no concentration in rays. As shown in Figure 11, their calculated density of scattered secondaries is in the lower range of the observed numbers reported by *Preblich et al.* [2007] inside the rays, but as much as 3 times higher than the observed numbers of "field secondaries" actually observed outside rays. This is important, because it may have contributed to the view of *McEwen et al.* [2005], and *Preblich et al.* [2007] argued that Zunil field secondaries are more numerous than we expect and lead to enormous errors in crater retention age. As we argued in section 2.4, however, (1) crater counters such as our group try to identify rays and exclude ray-covered areas from their counts; (2) as seen in Figure 11 the empirical counts by us at Gratteri and by *Preblich et al.* at Zunil show that the observed counts between ray systems typically run well below densities of field secondaries predicted in the simulation by *McEwen et al.* [2005]; (3) Figure 11 shows that beyond $\sim 150\text{--}200$ km from Gratteri ($\sim 20\text{--}30D_{\text{primary}}$), the counts of craters between rays remains relatively constant with distance, suggesting that secondaries emanating from Gratteri are not the main component of craters at that distance because we expect secondaries to be less numerous with distance [*Melosh*, 1984].

The results of *McEwen et al.* [2005], *Preblich et al.* [2007], and ourselves thus indicate that the largest concentrations of secondaries are inside the rays, while densities of field secondaries outside rays, while significant, are relatively low.

6. Dynamical Analysis

6.1. Estimates of Projectiles Size for Secondary Craters

The investigation of emplaced ejecta is a major issue in cratering mechanics. The ejecta emplacement is dependent on the interaction between the atmosphere and outward moving ejecta curtain that causes a difference between ejecta emplacement on the Moon and on planets with atmospheres [e.g., *Schultz and Gault*, 1979; *Shuvalov*, 2003]. *Schultz and Gault* [1979] suggested that drag-free conditions are generated around the transient crater at a very early stage of an impact event as the gases of the vaporized target and projectile expand. In a later stage of impact crater development the ejecta curtain generates an outward moving ring vortex of strong winds, which entrain small ejecta particles [*Barnouin-Jha and Schultz*, 1996]. According to the numerical simulations, which treat the ejecta as a large number of discrete particles interacting with the gas flow by momentum exchange [*Shuvalov*, 2003], particles smaller than about 10 cm dominate the intensive interaction with expanding vapor, while large particles are not subjected to action of expanding vapor [*Shuvalov et al.*, 2001; *Shuvalov*, 2003].

We estimated sizes and velocities of blocks forming the secondaries that we counted around Gratteri. These secondaries are formed by blocks roughly 1–20 m in size ejected with 0.3–1.5 km/s velocities. These values do not contradict to commonly used assumptions. We consider the emplacement of large blocks of material (larger than about dozens of centimeters in size), and we assume that these blocks are not influenced by expanding vapor and are moving through undisturbed atmosphere. Martian atmosphere is thick enough to decelerate stones smaller than a few meters in size [*Popova et al.*, 2003], so we take into account the deceleration of projectiles creating secondary craters.

We accept the following relations for crater sizes in gravity and strength regimes, respectively [*Ivanov*, 2001]

$$D = 1.16(\delta/\rho)^{1/3}d^{0.78}(V\sin\alpha)^{0.43}g^{-0.22} \quad (2)$$

and

$$D = 1.21(\delta/\rho)^{0.43}d(V\sin\alpha)^{0.55}(gD_{\text{sg}})^{-0.28} \quad (3)$$

where D is the crater diameter (m), d is the projectile diameter (m), V is the impact velocity (m/s), δ and ρ are meteoroid and target densities, α is the angle from horizontal, and g is the gravity acceleration (3.74 m/s^2 for

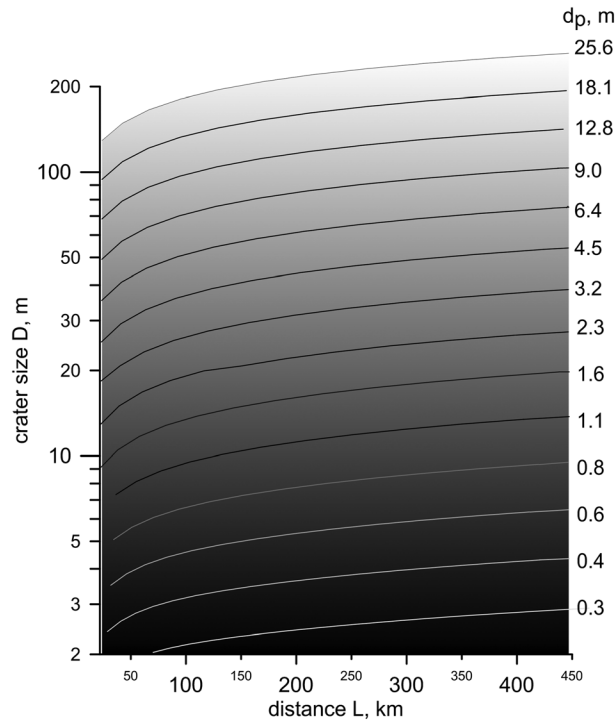


Figure 12. Projectile size dependence on distance from primary and crater diameter.

et al. [2014] used similar procedure and obtained inferred velocities as low as 70 m/s. Recent study of lunar secondaries [Singer *et al.*, 2013] offers insights into lunar impact ejecta physics from high-resolution mapping of secondary craters. They demonstrated that small secondaries still form with velocities as low as 50 m/s [Singer *et al.*, 2013]. At lower velocity events much of the impact energy is going into work against material strength. Vickery [1986] estimated the transition velocity for crater formation as 100–150 m/s. The simplest theoretical way to estimate the velocity at which the craters are starting to form is to compare the pressure at the impact point (very roughly $\sim \delta V^2$), with the dynamical strength of material. Assuming the projectile density $\delta \sim 3 \text{ g/cm}^3$ and the dynamical strength of silicates about 100 MPa, we may estimate that the transition velocity is about 170 m/s, slightly larger than her estimates. Hartmann [1967b] conducted Hawaiian field studies in an area of loose, centimeter-scale volcanic cinders, into which a nearby cinder cone had ejected boulders, producing “secondary” craters. In this loose material, many of the boulders had buried themselves, producing ordinary craters with raised rims up to 1.5 m across, but in other cases, the boulders were lying partially or entirely exposed in the crater centers suggesting that the impact velocities were near, but somewhat below, the effective mean transition velocity to make ordinary-looking “secondary” craters in that loose material. Citing observations of the eruption, Hartmann estimated the typical impact velocity at 75 m/s, not inconsistent with the above theoretical results for transition velocities. Ejection angle may vary at some extent, but we will assume an average value of 45° [Melosh, 1984]. We model the flight of differently sized ejected blocks (from submeter to few decameter sizes) with different ejection velocities taking into account the atmospheric deceleration and determined crater sizes according equations 2–4. The ablation was included in the consideration (as in Popova *et al.* [2003]), but it has negligible effect at considered low velocities. Initial ranges of block sizes and ejection velocities were adopted to cover the considered area around Gratteri craters (30–450 km from primary) and diameters of secondary craters, which were counted (1–100 m, Figure 8). The dependence of crater size on distance to the primary obtained for different size of ejecta block and ejecta velocities allows us to estimate the sizes of secondary crater forming projectiles (Figure 12). For example, a 20 m secondary crater, found at about 30 km distance, would have been created by a projectile ~ 3 m in diameter, whereas at 200 km distance, a projectile of 2 m would have been enough to make it.

The model data also allow to determine the ejection and impact velocity of the block, which forms differently sized secondaries at given distance. The deceleration plays a role for submeter and few meter blocks. For

Mars). D_{sg} is the diameter of transition between gravity and strength scaling, which Ivanov [2001] gives as being of order 100 m on Mars and 300 m on the Moon. The transition is not well defined and spreads over a range of diameters depending, for instance, on material. McEwen *et al.* [2005] use the range of 130–260 m; we adopt 200 m, which roughly corresponds to target strength of about 3 MPa.

The strength to gravity transition is incorporated into the scaling law [Ivanov, 2001] as follows:

$$\frac{D}{d(\delta/\rho)^{0.43}(V\sin\alpha)^{0.55}} = \frac{1.21}{[(D_{sg} + D)g]^{0.28}} \quad (4)$$

Crater size decreases with the impact velocity and below some critical velocity; blocks falling at low velocity will not create an explosive crater. Vickery [1986] studied secondary craters and derived projectile size and velocity. The inferred velocities vary from 0.2 km/s up to 1 km/s. Hirase

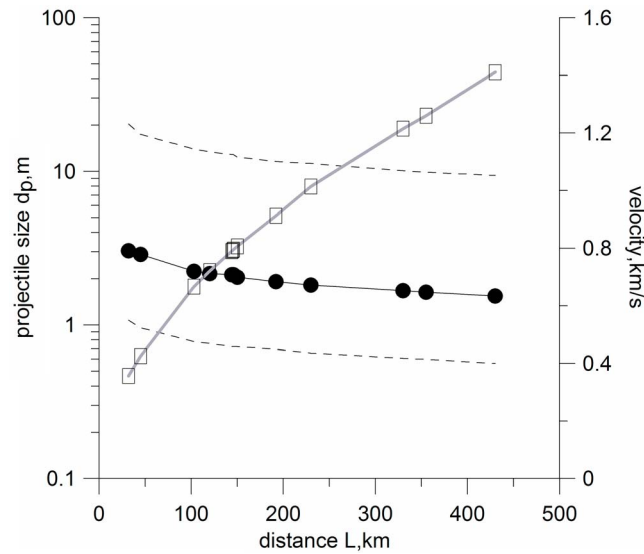


Figure 13. The size of projectiles forming secondary craters in 16–22 m bin versus distance from primary (black circles); ejection velocity for these blocks (grey curve with open squares). Projectile sizes for smallest (8–11 m) and largest (62–88 m) considered crater bins are marked by dashed lines.

by projectiles of about 1–6 m, ejected with velocities 0.3–1.5 km/s. The size of blocks slightly decreases with distance (Figure 13), indicating that the debris with highest launch velocity tends to be smaller than slower debris assuming the same ejection angle.

We inferred the projectile sizes from measured secondary crater sizes at different distances based on our modeling. These values could be compared with commonly used ejecta fragment size estimates. The size of the fragments ejected from the primary crater at a given point depends on the material properties and on the cratering process itself. The size distribution of solid fragments in high-velocity impacts has been estimated based on crater observations, from explosion experiments, and theoretically (for more details, see Artemieva and Ivanov [2004] and McEwen et al. [2005]). Several simplified approaches, which resulted in diverse fragment size distributions, are widely used [Artemieva and Ivanov, 2004]. For example, if the fragments occur under loading at constant strain rate (strain of the order ~0.1–0.01), their size and distribution are determined according Grady-Kipp theory [1980]. Melosh [1984] suggested that preferable size of fragments is about

$$L_{gk} = \frac{\sigma_t d}{\rho v_{ej}^{2/3} V^{1/3}} \tag{5}$$

where σ_t is the tension at fracture (~0.1 GPa for basalt and other igneous rocks), d is projectile diameter, V is the impact velocity, and v_{ej} is the ejection velocity. For ejection velocities of 0.3–1.5 km/s the calculated size of fragments is about 1.2–3.6 m just in the range of our estimates. The maximal size of Grady-Kipp fragments is about 7–23 m. Alternatively, the standard power law fragment distribution may be used assuming the size of largest block. This size from the entire crater $L_{max-max(m)}$ depends on crater size D (in km):

$$L_{max-max} = (25 \pm 12) D^{0.69} \tag{6}$$

[Ivanov and Basilevsky, 1983]. The size of most numerous ejecta blocks with any particular velocity may be found as $L_{max} = L_{max-max} (V_R/V_{ej})$, where V_R is an ejecta velocity near the transient crater rim. In this case the most numerous blocks ejected with velocities 0.3–1.5 km/s are about 3.6–18 m. In this approach smaller blocks are more common than large ones due to assumed power law distribution. Both approaches predict similar largest fragment size in the same range as we observed.

6.2. Total Mass of Ejecta Forming Secondaries

Gratteri crater is formed in the gravity regime, and the corresponding projectile diameter is about 680 m assuming projectile density $\delta \sim 2 \text{ g/cm}^3$, typical impact velocity of 10 km/s, and an impact angle of $\alpha = 45^\circ$.

blocks larger 5.5 m it decreases the impact velocities less than 5% (in considered range of ejection $V \sim 0.2\text{--}2 \text{ km/s}$). The corresponding impact velocities were larger than 150 m/s. Secondary craters we counted generally have sizes of about 1–100 m and are mostly at 30–500 km distance from the primary (Figure 8). We thus estimate that they are formed mainly at impact velocities 0.3–1.5 km/s.

The highest crater density is measured in the 16–22 m crater bin (Figure 8), and the corresponding projectile sizes versus distance is shown in Figure 13 as well as projectile size in largest and smallest crater size bins. The ejection velocities for blocks forming 16–22 m craters are shown. For the whole distance range (32–450 km) we may estimate that the most numerous are craters in the range 8–43 m, i.e., formed

According to crater ejecta scaling laws [Housen and Holsapple, 2011], the mass $M_{ej}(V)$ ejected from the crater faster than V_{ej} may be estimated in terms of crater radius R for crater in the gravity regime:

$$\frac{M_{ej}(V)}{\rho R^3} = C_5 \left\{ \frac{V_{ej} \sin \alpha}{\sqrt{gR}} \right\}^{-3\mu} \quad (7)$$

where C_5 and μ are constants. The excavated material with velocities in the range 0.2–5 km/s (larger than the transition velocity mentioned above, smaller than the escape velocity) is able to produce secondaries. For a reasonable value of power constant $\mu \sim 0.55$ for rocky target and $C_5 \sim 0.4$ [Housen and Holsapple, 2011] this amount is about 50% of crater volume. Secondaries, which we have counted (Figure 8), were produced by blocks with estimated ejection velocities of about 0.3–1.5 km/s (paragraph 6.1). The corresponding amount of material is about 23% of total volume or about $20m_p$, where m_p is the projectile mass. The numerical modeling of the Zunil estimated the amount of high-velocity solid ejecta ($V_{ej} > 1$ km/s) as $\sim 5\%$ of total ejecta volume [McEwen et al., 2005], whereas the equation above provides about 4%.

This amount of material ($\sim 20m_p$) is able to form about $\sim 10^8$ to $\sim 10^9$ secondaries by fragments 1–3 m in size under assumption that only fragments of these sizes are formed. That is an upper estimate as any other fragment size distribution will decrease the number of formed secondaries. Uniformly distributed 2 m fragments will produce about 14 craters/km² in the area from 32 to 400 km from primary. Being concentrated in the rays, which occupied 2.5% of the area, these craters will add about 500 craters/km². But, according to Table 2 the average fraction of secondaries inside the ray is about 20–40% and decreases the additional crater density inside the rays down to 150 craters/km² and provides about 6 craters/km² outside the rays. The measured crater density is on average 80 craters/km² in the rays and about 5 craters/km² in between. The measured density includes both background craters and Gratteri secondaries. So the rough estimates given above probably overestimated the number of secondaries but are in the same order of magnitude.

We may estimate an upper limit on the amount of ejecta based on measured crater densities by assuming that all observed craters are secondaries. The mass and velocity of fragments forming secondaries are estimated with the help of Figure 12. The total mass of ejected material forming rays is about 1% of estimated ejected mass ($20m_p$ with velocity 0.3–1.5 km/s), whereas between the rays there are about 18%. The total amount of mass we obtained is 5 times smaller than the estimates based on equation (7). One possible reason for this disagreement may be real fragment size distribution of secondary projectiles with large number of smaller particles, in which craters could not be counted with high precision or even are decelerated by the Martian atmosphere. The uncertainty in crater scaling relation also could add a factor of 2 or 3. The other assumptions we made that may affect this result are that the area of rays is estimated very roughly, that the measured densities cover only small part of the rays, and that the densities could vary from ray to ray. The relations between ejected mass in rays and outside rays is about 1:18 (see section 6), that is much larger than the relation 3:7 we got in Table 2.

7. Implication for Crater Count Chronology

It has been argued that secondaries fatally “contaminate,” or at least threaten the integrity of, crater chronometry efforts, because secondaries are created nonrandomly in space and time [McEwen et al., 2005; McEwen and Bierhaus, 2006]. This statement seems decisive at first glance, but the practical consequences are less clear when examined carefully. To consider the nonrandomness in space, we find that the rays are well defined by crater clusters and alignments out to about 450 km from Gratteri, and thus are likely to be excluded from crater counts, since both Hartmann and Neukum, for example, have stated that, in effect, they draw a “box” around suspect clusters and rays and remove those areas from their counts. According to our data on Gratteri, that technique removes at least 20–40% of the secondaries generated by Gratteri out to those distances, since about 20–40% of the secondaries are inside rays and the other secondaries are scattered at low densities in the spaces between rays. The remaining issue is whether those low, interray densities of secondaries have much effect on crater-count age estimates. Figures 7e and 7f show that at secondary crater diameters ~ 8 m to ~ 31 m diameter, the crater density of Gratteri secondaries (S) cannot be higher than about 9 to 1 crater/km², respectively (the values measured for background primaries plus field secondaries, $P + S$). Examining the template isochron diagrams in Figure 7, we see that the time interval to produce these respective densities for craters in this 8–31 m size range is ~ 1 to ~ 100 Ma. That suggests that, within

conservative limits, if Gratteri-like craters are formed on Martian surfaces older than the last few percent of the age of Mars, the “contaminating” counts of new secondaries *between the rays* from the new crater will be overwhelmed by the preexisting P+S background counts and have little effect on crater chronometry.

The nonrandomness in time is still more complex. Consider a random site on Mars and the history of secondary decameter-scale craters accumulating at that site from “off-stage” primaries. *McEwen et al.* [2005] pointed out that a Zunil-sized (10 km diameter) impact crater should form roughly once per 1 Myr and is big enough to scatter field secondaries over much of Mars. Our team derived crater retention ages for Zunil of about 0.06 to 1 Myr based on counts of few craters inside Zunil and on its ejecta blanket and using both Neukum and Hartmann isochron systems [*Hartmann et al.*, 2010]. In general, the minimum size of crater sufficient to scatter craters around Mars corresponds to the minimum size need to eject potential Martian meteorites from Mars at escape velocity. On theoretical grounds, and on combined theoretical/empirical grounds involving shock pressures, this size has been estimated to be “as small as ~3 km” [*Head et al.*, 2002]. *Beck et al.* [2005] infer a crater size of 1.5 to 4.0 km for the Martian crater that launched the Zagami shergottite. However, others authors claim that all shergottites could have been launched from the 58 km rayed crater Mojave [*Werner et al.*, 2014]. Purely empirically, we note that all measured cosmic ray exposure age estimates for Martian meteorites range between about 0.5 to 20 Ma. For the different type shergottites these exposure ages lie between 0.73 and 18 Ma; for ALH84001 it is 14.2 Ma, and for a cluster of nakhalite/chassignites, at ~11.0 Myr [*Herzog and Caffee*, 2014]. Our team studied six other young Martian craters with detectable broad infrared rays, with diameters from 2.6 to 29 km, and derived ages in the range of 0.1 to 30 Myr [*Hartmann et al.*, 2010]. Thus, loosely, we can estimate the timescale of the most recent global-scale showers of secondary impact craters as roughly million year intervals. From these data we suggest that for any chosen “test surface” younger than about 50,000 years there probably have not been global showers of small secondaries, and any field secondaries would come from relatively nearby small primaries, perhaps of 1 km scale, and only a few tens of km away. Again, there is a “maximum danger zone” for crater retention ages of any surfaces estimated to have ages around 50,000 years to 10 Myr, because we are not sure if zero, one, or even several off-stage, distant, Zunil-class primaries have contributed a shower of decameter class field secondaries onto the area being studied, although we should detect these craters from the presence of rays. *Tornabene et al.* [2006] and *Werner et al.* [2014] could jointly detect no more than 30 of such craters. Thus, as emphasized by *McEwen et al.* [2005], *Daubar et al.* [2013], and *Hartmann et al.* [2014], the estimated error bar on any age in this time interval is large. Even in that most uncomfortable situation, however, we can get a meaningful and useful upper limit on age, simply by assuming (in the extreme case) that no secondaries have formed, so that all visible decameter-scale craters are primaries [*Hartmann et al.*, 2014], using the increasingly well-known primary formation rates from [*Daubar et al.*, 2013, 2014]. As we move to surfaces with ages > 10 Myr, we gain increasing confidence, because something on the order of 10 “Zunils” will have formed on Mars (note from the Mars meteorites) so that a given test area on Mars has been subjected to roughly 10 showers from “Zunils” in different directions and at different distances. For surfaces older than 20 Myr, we would argue that the nonrandomness-in-time problem disappears because the overlapping secondary fields become more randomized. Also, the difference between 19 showers and 20 showers from distant “Zunils” is less than the current uncertainty in the crater chronometry systems. Thus, for surfaces in the age range from 10 or 20 Myr up to 100 Myr, we believe that crater counts on decameter-scale craters can give valuable results. (Note, for example, that the last few obliquity excursions beyond 45° occurred over some tens of Millions years prior to 5.5 Myr ago and may have involved observable excursions in climate and ice deposition at certain Martian locations [*Hartmann et al.*, 2014]). Interestingly, for surfaces older than ~200 Myr (most of Martian history!), the problem of using decameter-scale secondaries surface becomes moot, because craters of $D < \sim 30$ m become saturated, and we must appeal to larger than an increasingly large diameter limit to derive age information. The implications for temporal nonrandomness, then, is that there is a “danger zone” for crater chronometry that peaks for ages of roughly 50,000 years to 10 Myr.

8. Conclusions

We studied the secondary crater field of the young Martian primary ray crater Gratteri (diameter 7 km). We identified an unusual class of craters we call “rampart secondaries” with dissymmetric geometry matching with ejection from Gratteri. We also measured size distributions of secondaries as a function of distance from

Gratteri and used these data to reconstruct the mass-velocity distribution of ejecta blasted out of Gratteri. Our result indicated that crater density in rays tends to peak around 120–230 km from Gratteri (roughly 20–30 D_{primary}) and reaches roughly 30–70 times the interray crater density. We emphasize from observations and dynamical analysis that about half of secondaries are concentrated inside the rays. The large-scale background topography dates from the Noachian and Hesperian periods, but at the size of the secondaries (mostly $D < \sim 60$ m), craters and other topographic features survive only from the Amazonian, which shows that the entire SFD must be utilized in order to interpret the history of a Martian region. These results along with measurements of the current impact rate on Mars tend to rule out interpretations that the mere existence of secondaries destroys the effectiveness of the crater counting techniques for age determination. Because the crater SFDs on Mars range over 4 orders of magnitude in crater density, we believe that counts of primaries plus field secondaries (P + S) give useful chronometric and geophysical information, meaningfully distinguishing geologic formations formed in the last millions of years from the oldest geologic formations, dating from several gigayears ago.

Acknowledgments

The data for this paper are available at NASA Planetary Data System Archive (<http://pds.nasa.gov/>). We used the images of the following instruments: MOC, THEMIS, and HiRISE. We thank the International Space Science Institute in Bern, Switzerland, for hosting our several workshop meetings and facilitating our work. We also thank European Research Council for the funding of two workshop meetings at University of Lyon, France (FP7/2007-2013/ERC grant agreement 280168). Hartmann acknowledges support from the NASA Mars Data Analysis Program. S.C. Werner is supported by the Research Council of Norway through the CRATER CLOCK project (235058) and through the Centre of Excellence funding scheme, project 223272 (CEED). Thanks to Emily Joseph and Dan Berman, at the Planetary Science Institute, for assisting in image production and several of the crater counts.

References

- Anderson, J. L. B., P. H. Schultz, and J. T. Heineck (2003), Asymmetry of ejecta flow during oblique impacts using three-dimensional particle image velocimetry, *J. Geophys. Res.*, *108*(E8), 5094, doi:10.1029/2003JE002075.
- Artemieva, N., and B. Ivanov (2004), Launch of Martian meteorites in oblique impacts, *Icarus*, *171*, 84–101.
- Barnouin-Jha, O. S., and P. H. Schultz (1996), Ejecta entrainment by impact-generated ring vortices: Theory and experiments, *J. Geophys. Res.*, *101*, 21,099–21,116, doi:10.1029/96JE01949.
- Beck, P., P. Gillet, A. El Goresy, and S. Mostefaoui (2005), Timescales of shock processes in chondritic and Martian meteorites, *Nature*, *435*, 1071–1074.
- Bierhaus E. B., C. R. Chapman, and W. J. Merline (2005), Secondary craters on Europa and implications for cratered surfaces, *Nature*, *437*, 1125–1127, doi:10.1038/nature04069.
- Calef, F. J., R. R. Herrick, and V. L. Sharpton (2009), Geomorphic analysis of small rayed craters on Mars: Examining primary vs. secondary impacts, *J. Geophys. Res.*, *114*, E10007, doi:10.1029/2008JE003283.
- Chapman, C. (1968), Interpretation of the diameter-frequency relation for lunar craters photographed by Rangers VII, VIII, and IX, *Icarus*, *8*, 1–22.
- Chapman, C., J. Pollack, and C. Sagan (1969), An analysis of the Mariner 4 photography of Mars, *Astron. J.*, *74*, 1039–1051.
- Chapman, C. R. (1974), Cratering on Mars. I. Cratering and obliteration history, *Icarus*, *22*, 272–291.
- Chapman, C. R. (2004), Mars cratering issues: Secondary cratering and end-Noachian degradation. In *Second Conference on Early Mars: Geologic, Hydrologic, and Climatic Evolution and the Implications for Life* [CD-ROM], Abstract 8028, Lunar and Planetary Institute, Houston, Tex.
- Chapman, C. R., and K. Jones (1977), Cratering and obliteration history of Mars, *Ann. Rev. Earth. Planet. Sci.*, *5*, 515–540.
- Daubar, I. J., A. McEwen, S. Byrne, M. R. Kennedy, and B. Ivanov (2013), The current Martian cratering rate, *Icarus*, *225*(1), 506–516, doi:10.1012/j.icarus.2013.04.009.
- Daubar, I. J., A. S. McEwen, S. Byrne, M. Kreslavsky, L. Saper, and M. R. Kennedy (2014), New dated impacts on Mars and an updated current cratering rate, 8th Int. Conf. on Mars, July 14–18, Pasadena, CA, USA, LPI Contributions 1791, Abstract 1007.
- Forget, F., R. M. Haberle, F. Montmessin, B. Levrard, and J. W. Head (2006), Formation of glaciers on Mars by atmospheric precipitation at high obliquity, *Science*, *311*, 368–371.
- Gault, D., and J. A. Wedekind (1978), Experimental studies of oblique impact, Proc. Lunar Planet. Sci. Conf. 9th, 3843–3875.
- Grady, D. E., and M. E. Kipp (1980), Continuum modeling of explosive fracture in oil shale. Int. J. Rock, 729 Mech. Min. Sci. Geomech. Abstract 17, 147–157.
- Hartmann, W. K. (1966), Martian cratering, *Icarus*, *5*, 565–576.
- Hartmann, W. K. (1967a), *Lunar Crater Counts. I: Alphonsus*, vol. 6, pp. 31–38, Commun. Lunar Planetary Lab., Tucson.
- Hartmann, W. K. (1967b), Secondary volcanic impact craters at Kapoho, Hawaii, and comparisons with the lunar surface, *Icarus*, *7*, 66–75.
- Hartmann, W. K. (1970), Lunar cratering chronology, *Icarus*, *13*, 209–301.
- Hartmann, W. K. (1971), Martian cratering III: Theory of crater obliteration, *Icarus*, *15*, 410–428.
- Hartmann, W. K. (1972), Paleocratering of the Moon: Review of post-Apollo data, *Astrophys. Space Sci.*, *12*, 48–64.
- Hartmann, W. K. (2005), Martian cratering 8: Isochron refinement and the chronology of Mars, *Icarus*, *174*, 194–320.
- Hartmann, W. K. (2007), Martian cratering 9: Toward resolution of the controversy about small craters, *Icarus*, *189*, 274–278.
- Hartmann, W. K., and N. Barlow (2006), Nature of the Martian uplands: Effect on Martian meteorite age distribution and secondary cratering, *Meteor. Planet. Sci.*, *41*, 1453–1467.
- Hartmann, W. K., and G. Neukum (2001), Cratering chronology and the evolution of Mars, *Space Sci. Rev.*, *96*, 165–194.
- Hartmann, W. K., et al. (1981), Chronology of planetary volcanism by comparative studies of planetary craters, in *Basaltic Volcanism on the Terrestrial Planets*, pp. 1050–1127, Pergamon Press, Elmsford, N. Y.
- Hartmann, W. K., M. Malin, A. McEwen, M. Carr, L. Soderblom, P. Thomas, E. Danielson, P. James, and J. Veverka (1999), Evidence for recent volcanism on Mars from crater counts, *Nature*, *397*, 586–589.
- Hartmann, W. K., C. Quantin, S. Werner, and O. Popova (2010), Do young Martian ray craters have ages consistent with the crater count system?, *Icarus*, *208*, 621–635.
- Hartmann, W. K., V. Ansan, N. Mangold, D. Berman, and F. Forget (2014), Comprehensive analysis of glaciated Martian Crater Greg, *Icarus*, *228*, 96–120, doi:10.1016/j.icarus.2013.09.016.
- Head, J. N., H. J. Melosh, and B. A. Ivanov (2002), Martian meteorite launch: High-speed ejecta from small craters, *Science*, *298*, 1752–1756.
- Herrick, R. R., and K. K. Hessen (2006), The planforms of low-angle impact craters in the northern hemisphere of Mars, *Meteoritics Planet. Sci.*, *41*, 1483–1495.
- Herzog, G. F., and M. W. Caffee (2014), Cosmic-ray exposure ages of meteorites, in *Treatise on Geochemistry*, 2nd ed., edited by H. D. Holland and K. K. Turekian, pp. 419–454, Elsevier, Amsterdam.
- Hirase, Y., A. Nakamura, and T. Michikami (2014), Ejecta size-velocity relation derived from the distribution of the secondary craters of kilometer-sized craters on Mars, *Planet. Space Sci.*, *52*(12), 1103–1108.

- Hirata, N., and Nakamura A. K. (2006), Secondary craters of Tycho: Size-frequency distributions and estimated fragment size-velocity relationships, *J. Geophys. Res.*, *111*, E03005, doi:10.1029/2005JE002484.
- Hodges, C. A., and D. E. Wilhelms (1977), Formation of lunar basin rings, *Icarus*, *34*, 294–323.
- Housen, K. R., and K. A. Holsapple (2011), Ejecta from impact craters, *Icarus*, *211*(1), 856–875, doi:10.1016/j.icarus.2010.09.017.
- Ivanov, B. A. (2001), Mars/Moon cratering rate ratio estimates, in *Chronology and Evolution of Mars*, edited by R. Kallenbach, J. Geiss, and W. K. Hartmann, pp. 87–104, International Space Science Institute, Bern.
- Ivanov, B. A., and A. T. Basilevsky (1983), On the fragment-size distribution of ejecta of impact craters, LPSC XIV, 345.
- Ivanov, B. A., H. J. Melosh, and A. S. McEwen (2009), Small impact crater clusters in high resolution HiRISE images, LPSC 40, abstract 1410.
- Jones, K. L. (1974), Evidence for an episode of crater obliteration intermediate in Martian history, *J. Geophys. Res.*, *79*, 3917–3931, doi:10.1029/JB079i026p03917.
- Kite, E. S., A. Lucas, and C. I. Fassett (2013), Pacing early Mars river activity: Embedded craters in the Aeolis Dorsa region imply river activity spanned \geq (1–20) Myr, *Icarus*, *225*, 850–855.
- Malin, M. C., et al. (1998), Early views of the Martian surface from the Mars Orbiter Camera of Mars Global Surveyor, *Science*, *00368075*, 3/13/1998, 279(5357), 1681–1685.
- Malin, M. C., K. S. Edgett, L. V. Posiolova, S. M. McColley, and E. Z. N. Dobra (2006), Present-day impact cratering rate and contemporary gully activity on Mars, *Science*, *314*, 1573–1577, doi:10.1126/science.1135156.
- McEwen, A. S., and E. B. Bierhaus (2006), The importance of secondary cratering to age constraints on planetary surfaces, *Annu. Rev. Earth Planet. Sci.*, *34*, 535, doi:10.1146/annurev.earth.34.031405.125018.
- McEwen, A. S., B. S. Preblich, E. P. Turtle, N. A. Artemieva, M. P. Golombek, M. Hurst, R. L. Kirk, D. M. Burr, and P. R. Christensen (2005), The rayed crater Zunil and interpretations of small impact craters on Mars, *Icarus*, *1976*, 351–381.
- Melosh, H. J. (1984), Impact ejection, spallation, and the origin of meteorites, *Icarus*, *59*, 234–260.
- Neukum, G. (1983), Meteoritenbombardement und Datierung planetarer Oberflächen, Habilitation Dissertation for Faculty Membership, Ludwig-Maximilians Univ. München, Munich, Germany, 186 pp.
- Neukum, G., and B. A. Ivanov (1994), Crater size distribution and impact probabilities on Earth from lunar, terrestrial-planet, and asteroid cratering data, in edited by T. Gehrels, *Hazards Due to Comets and Asteroids*, pp. 359–416, Univ. Arizona Press, Tucson.
- Neukum, G., and B. König (1976), Dating of individual lunar craters. Proc. Lunar Sci. Conf. 7th pp. 2867–2881.
- Neukum, G., B. König, and J. Arkani-Hamed (1975a), A study of lunar impact crater size distributions, *Moon*, *12*, 201–229.
- Neukum, G., B. König, B. Storzer, D., and H. Fechtig (1975b), Chronology of lunar cratering, *Proc. 6th Lunar Planet. Sci. Conf.* 598 (abstract).
- Neukum, G., B. A. Ivanov, and W. K. Hartmann (2001), Cratering records in the inner solar system in relation to the lunar reference system, *Space Sci. Rev.*, *96*, 55–86.
- Öpik, E. J. (1964), Mariner IV and craters on Mars, *Ir. Astron. J.*, *6*, 308.
- Öpik, E. J. (1965), Mariner IV and craters on Mars, *Ir. Astron. J.*, *7*, S92–S104.
- Öpik, E. J. (1966), The Martian Surface, *Science*, *153*, 255–265.
- Plescia, J. B. (2005), Small-diameter Martian craters: Applicability for chronology—or not. Lunar Plan. Sci. Conf. Abstract 2171.
- Popova, O., I. Nemtchinov, and W. K. Hartmann (2003), Bolides in the present and past Martian atmosphere and effects on cratering processes, *Meteorit. Planet. Sci.*, *38*(6), 905–925.
- Popova, O., W. K. Hartmann, I. V. Nemtchinov, D. C. Richardson, and D. C. Berman (2007), Crater clusters on Mars: Shedding light on Martian ejecta launch conditions, *Icarus*, *190*, 50–73.
- Preblich, B. S., A. S. McEwen, and D. M. Studer, 2007, Mapping rays and secondary craters from the Martian Crater Zunil, *J. Geophys. Res.*, *112*, E05006, doi:10.1029/2006JE002817.
- Quantin, C., N. Mangold, W. K. Hartmann, and P. Allemand (2007), Possible long-term decline in impact rates 1: Martian geological data, *Icarus* (IP:3.34), *186*(1), 1–10.
- Robbins, S. J., and B. M. Hynek (2011a), Distant secondary craters from Lyot crater, Mars, and implications for the surface ages of planetary bodies, *Geo. Res. Lett.*, *38*, L05201, doi:10.1029/2010GL046450.
- Robbins, S. J., and B. M. Hynek (2011b), Secondary crater fields from 24 large primary craters on Mars: Insights into nearby secondary crater production, *J. Geophys. Res.*, *116*, E10003, doi:10.1029/2011JG003820.
- Schultz, P. H., and D. E. J. Gault (1979), Atmospheric effect on Martian ejecta emplacement, *J. Geophys. Res.*, *84*, 7669–7687, doi:10.1029/JB084iB13p07669.
- Schultz, P. H., and Singer J. (1980), A comparison of secondary craters on the Moon, Mercury, and Mars. Proc. Lunar Sci Conf.11, 2243–2259.
- Schultz, P. H., C. A. Eberhardy, C. M. Ernst, M. F. A'Hearn, J. M. Sunshine, and C. M. Lisse (2007), The Deep Impact oblique impact cratering experiment, *Icarus*, *190*, 295–333, doi:10.1016/j.icarus.2007.06.006.
- Shoemaker, E. M. (1965), Preliminary analysis of the fine structure of Mare Cognitum. Jet Propulsion Laboratory, Californian Institute of Technology, *Tech. Rept.*, 32–700(1965), 75–134.
- Shoemaker, E. M., M. H. Hait, G. A. Swann, D. L. Schleicher, D. H. Dahlem, G. G. Schaber, and R. L. Sutton (1970), Lunar regolith at Tranquillity Base, *Science*, *167*, 452–455.
- Shuvalov, V. (2003), Cratering process after oblique impacts, Third international Conference on Large Meteorite Impacts, Nördlingen, contribution 4130.
- Shuvalov, V. (2012), A mechanism for the production of crater rays, *Meteorit. Planet. Sci.*, *47*, 262–267, doi:10.1111/j.1945-5100.2011.01324.x.
- Shuvalov, V., H. Dypvik, and F. Tsikalas (2001), Numerical simulations of the Mjølner marine impact: In Smelror, M., Dypvik, H. and Tsikalas, F. (eds) "Submarine Craters & Ejecta-Crater Correlation [7th Workshop, European Science Foundation (ESF)-IMPACT Programme], *Norwegian Geological Society Abstracts & Proceedings*, No 1, p. 73–75.
- Singer, K. N., W. B. McKinnon, and B. L. Jolliff (2013), Secondary craters and the size-velocity distribution of ejected fragments around lunar craters measured using LROC images, *AGU Abstract P41F-1976*.
- Tanaka, K. L., J. A. Jr., Skinner, J. M. Dohm, R. P. III Irwin, E. J. Kolb, C. M. Fortezzo, T. Platz, G. G. Michael, and T. M. Hare (2014), Geologic map of Mars, *U.S. Geol. Surv. Sci. Invest. Map*, *3292*, scale 1:20,000,000, pamphlet 43 p., 10.3133/sim3292.
- Tornabene L. L., J. E. Moersch, H. Y. Jr., McSween, A. S. McEwen, J. L. Piatek, K. A. Milam, and P. R. Christensen (2006), Identification of large (2–10 km) rayed craters on Mars in THEMIS thermal infrared images: Implications for possible Martian meteorite source regions, *J. Geophys. Res.*, *111*, E10006, doi:10.1029/2005JE002600.
- Vickery, A. M. (1986), Size-velocity distribution of large ejectas fragments, *Icarus*, *67*, 224–236.

- Werner, S. C., B. A. Ivanov, and G. Neukum (2009), Theoretical analysis of secondary cratering on Mars and an image-based study on the Cerberus Plains, *Icarus*, 200(2), 406–417, doi:10.1016/j.icarus.2008.10.011.
- Werner, S. C., A. Ody, and F. Poulet (2014), The source crater of Martian Shergottite Meteorites, *Science*, 343(6177), 1343–1346.
- Wilhelms, D. E. (1976), Secondary impact craters of lunar basins, Proc. Lunar. Sci. Conf., 7th, 2883–2901.